39.1 (sec.), 42.8 (sec.), 51.8 (quat.), 52.2 (tert.), 54.8 (tert.), 61.5 (quat.), 64.5 (quat.), 67.0 (tert.), 75.5 (quat.), 136.0 (olefinic), 139.3 (olefinic), 141.3 (olefinic), 144.1 ppm (olefinic.); MS (FAB, *m/z*) 294 [M$^+$]. Anal. Calcd for $C_{21}H_{26}O\cdot 1/4H_2O$: C, 84.37; H, 8.85%. Found: C, 84.49; H, 8.85%. **25**: colorless crystals (toluene), mp 69−71 °C; ^{1}H NMR δ 1.20 (d, J = 12.0 Hz, 1H), 1.28 (s, 1H), 1.35 (s, 1H), 1.41 (d, J = 12.0 Hz, 1H), 1.44−1.71 (m, 13H), 1.78−1.81 (m, 1H), 1.88−1.94 (m, 2H), 1.99−2.02 (m, 2H), 2.04 (d, J = 6.5 Hz, 1H), 2.06 (s, 2H), 2.14 (d, J = 6.5 Hz, 1H); ^{13}C NMR (DEPT) δ 19.5 (sec.), 29.4 (sec.), 30.4 (sec.), 35.4 (sec.), 36.4 (sec.), 36.8 (sec.), 37.8 (two sec.), 38.3 (tert.), 39.3 (sec.), 40.1 (sec.), 43.1 (quart.), 43.3 (quart.), 46.0 (tert.), 47.1 (tert.), 50.8 (tert.), 55.8 (quat.), 56.0 (quat.), 58.5 (quat.), 62.7 (tert.), 77.0 (quat.); MS (FAB, *m/z*) 294 (M$^+$). Anal. Calcd for $C_{21}H_{26}O\cdot 1/2H_2O$: C, 83.12; H, 8.97%. Found: C, 83.16; H, 8.94%.

(3) Photolysis of 2 in a Mixture of MeOH and 2 mol/L Aqueous HCl (17:1, v/v). A MeOH-2 mol/L HCl (17:1, v/v) solution (270 mL) of **2** (760 mg, 2.74 mmol) in a quartz vessel was irradiated with sterilizing lamps (10 W × 7) under Ar for 80 min at room temperature while monitoring the reaction by the ^{1}H NMR spectra in every 20 min. After removal of the solvent under reduced pressure, the residue was separated by recycle HPLC on GPC with $CHCl_3$ to afford polycyclic methoxy compound **26** (23 mg, 2.7%), polycyclic dimethoxy compound **27** (100 mg, 11%), and polycyclic methoxyhydroxy compound **28** along with the recovery of the starting **2** (80 mg, 11%). **26**: colorless oil. ^{1}H NMR δ 1.12 (d, J = 11 Hz, 1H), 1.23 (s, 1H), 2.17 (d, J = 11 Hz, 1H), 1.41−2.06 (m, 26H), 3.17 (s, 3H); ^{13}C NMR (DEPT) δ 19.9 (sec.), 30.1 (sec.), 30.9 (sec.), 33.4 (sec.), 36.2 (sec.), 37.0 (sec.), 37.1 (sec.), 37.3 (sec.), 38.4 (sec), 39.8 (sec.), 39.8 (tert.), 40.8 (sec.). 43.7 (quat.), 44.4 (quat.), 46.6 (tert.), 47.6 (quat.), 49.2 (quat.), 51.2 (tert.), 56.1 (quat.), 57.0 (quat.), 59.0 (quat.), 61.3 (prim.), 81.9 (quat.); HRMS (FAB, *m/z*) obsd. 308.2144 [M$^+$], calcd for 308.4637. **27**: mp 56−57 °C; ^{1}H NMR δ 1.03 (d, J = 13 Hz, 1H), 1.16 (d, J = 11 Hz, 1H), 1.26−1.78 (m, 20H), 1.90 (d, J = 11 Hz, 1H), 2.03 (d, J = 5.7 Hz, 1H), 2.26 (d, J = 13 Hz, 1H), 2.83 (s, 1H), 3.16 (s, 3H), 3.35 (s, 3H); ^{13}C NMR (DEPT) δ 19.9 (sec.), 25.0 (sec.), 26.1 (sec.), 32.1 (sec.), 34.0 (sec.), 35.4 (sec.), 36.5 (sec.), 36.6 (sec), 37.4 (sec.). 37.9 (sec.), 40.9 (sec.), 45.1 (tert.), 45.3 (tert.), 48.2 (quat.), 49.2 (quat.), 51.0 (tert.), 51.9 (quat.), 56.4 (quat.), 57.3 (quat.), 59.4 (prim.), 65.0 (prim.), 86.2 (quat.), 89.6 ppm (tert.). GC−MS (EI, *m/z*) 340 [M$^+$]. Anal. Calcd for $C_{23}H_{32}O_2\cdot 1/8H_2O$: C, 80.63; H, 9.39%. Found: C, 80.65; H, 9.33%. **28**: mp 138−139 °C; ^{1}H NMR δ 1.10 (d, J = 13 Hz, 1H), 1.19 (d, J = 12 Hz, 1H), 1.27−1.73 (m, 21H), 1.93 (d, J = 12 Hz, 1H), 2.07 (d, J = 4.2 Hz, 1H), 2.25 (d, J = 13 Hz, 1H), 3.18 (s, 3H), 3.32 (s, 1H); ^{13}C NMR (DEPT) δ 19.9 (sec.), 25.4 (sec.), 26.1 (sec.), 31.4 (sec.), 34.0 (sec.), 35.0 (sec.), 35.4 (sec.), 36.1 (sec.), 37.4 (two, sec.), 41.5 (sec.), 45.1 (tert.), 45.3 (tert.), 47.7 (quat.). 49.5 (quat.), 51.0 (tert.), 52.2 (quat.), 56.0 (quat.), 57.6 (quat.), 64.5 (prim.), 79.3 (tert.), 86.2 ppm (quat.). GC-MS (EI, *m/z*) 326 [M$^+$]. Anal. Calcd for $C_{23}H_{30}O_2\cdot 1/2H_2O$: C, 79.83; H, 9.28%. Found: C, 79.78; H, 9.13%

(4) Photolysis of 2 in Nonpolar Solvents. A dry hexane solution (500 mL) of **2** (700 mg, 2.52 mmol) in a quartz apparatus was irradiated with sterilizing lamps (10 W × 7) with continuous oxygen gas bubbling for 25 min at room temperature. The solvent was removed under reduced pressure, the residue was separated by PTLC (SiO_2; CH_2Cl_2), and then by HPLC (C18, MeOH). Very small amounts of **29** and **30** were isolated and identified by ^{1}H NMR and GC−MS. The yields of these compounds depend on the amount of dissolved oxygen in solution; **29** (0.8−1%) and **30** (0.6−0.7%). Irradiation of **2** (700 mg, 2.52 mmol) in acetone with high-pressure Hg lamp for 1 h gave the compounds **29** (2.7%) and **30** (1.2%) after the similar separation and purification procedure described above. **29**: yellow oil. ^{1}H NMR δ 7.01 (s, 1H), 6.78 (s, 2H), 6.65 (s, 1H), 6.37 (s, 2H), 2.54−3.12 (m, 16H); MS (FAB, *m/z*) 292 [M$^+$-H]. Anal. Calcd for $C_{21}H_{24}O$: $1.5H_2O$, C, 78.96, H, 8.52%. Found: C, 78.81, H, 8.28%. **30**: yellow oil. ^{1}H NMR δ 6.79 (s, 1H), 6.68 (s, 1H), 6.57 (s, 1H), 6.51 (s, 1H), 6.45 (s, 1H), 6.28 (s, 1H), 4.62 (s, 1H), 2.62−2.87 (m, 10H), 2.10−2.22 (m, 6H); MS (FAB, *m/z*) 291 [M$^+$]. Anal. Calcd for $C_{21}H_{22}O$: 0.65MeOH, C, 83.55; H, 7.97%. Found: C, 83.62; H, 8.01%.

(5) Photolysis of 2 in Acetone. A solution of **2** (400 mg, 1.45 mmol) in acetone (400 mL) was irradiated with a high-pressure Hg lamp (400 W) under argon for 14 h at room temperature while monitoring the reaction by ^{1}H NMR. After removal of the solvent under reduced pressure, the residue was purified by recycle HPLC on GPC type with CH_3Cl to afford 1-acetyl[3$_3$](1,3,5)cyclophane **31** (5 mg, 1.1%) along with the recovery of the starting material (114 mg, 29%). **31**: ^{1}H NMR ($CDCl_3$) δ 2.01 (s, −COMe, 3H), 2.19 (m), 2.68−2.74 (m), 3.00 (m), 6.39 (s, aromatic), 6.48−6.49 (m), 6.54−6.56 (m) ^{13}CNMR($CDCl_3$) δ 28.6, 28.8, 28.8, 30.0, 34.8, 36.8, 36.4, 36.5, 60.8, 127, 128, 130, 132, 133, 138, 140, 141, 141, 142, 208 ppm. MS (FAB, *m/z*) 332 [M$^+$], Anal. Calcd for $C_{24}H_{28}O\cdot 0.05$ benzene: C, 86.76; H, 8.48%. Found: C, 86.75; H, 8.52%.

Acknowledgment. T.S. gratefully acknowledge financial support by a Grant-in-Aid for Scientific Research (B) (No. 14340200) from the Ministry of Education, Culture, Sports, Science and Technology, Japan. T.S. sincerely thanks the financial support by the Shorai Foundation for Science and Technology, Japan.

Supporting Information Available: The alternative mechanism of single electron transfer (Scheme S1), crystal packing diagrams of compounds **24** and **31**(Figures S1, S2), and a summary of the crystallographic data and refinement details (Table S1). This material is available free of charge via the Internet at http://pubs.acs.org.

JA030032X

9-Fluoro-18-hydroxy-[3.3]metacyclophane: Synthesis and Estimation of a C–F···H–O Hydrogen Bond

Hiroyuki Takemura,*[a] Masayuki Kotoku,[b] Mikio Yasutake,[c][‡] and Teruo Shinmyozu[c]

Keywords: Hydrogen bonds / Fluorine / Cyclophanes / X-ray diffraction

A cyclophane composed of fluorobenzene and phenol units was synthesized in order to observe the C–F···H–O hydrogen bond. In the crystal structure, 20% of the molecule clearly shows the intramolecular hydrogen bond and the other 80% is free from hydrogen bonding. On the other hand, a distinct low-field shift of the phenolic OH proton was observed in the ^{1}H NMR spectrum compared to that of the F-free analog. Furthermore, O–H···F through-space coupling was observed. From the results of the crystallographic analysis, IR, and NMR spectra, the C–F···H–O hydrogen bond energy of this system was estimated to be 0.84–3.7 kJ·mol^{-1}.

Introduction

The C–F···H–X (X = O, N) hydrogen bonds are a new type of hydrogen bond, which was first proposed by Glusker et al. in 1983.[1] Following their work, research studies and discussions have been continued by many researchers who are still making efforts to confirm the hydrogen bonds using a variety of methods. This tendency indicates that CF···H–X hydrogen bonds are not widely distributed even in modern chemistry. Various methods are employed for the search, i.e., statistical methods utilizing a crystallographic database,[2,3] crystallographic analyses, spectroscopic methods,[4–9] and theoretical calculations.[10–12] Howard et al. adopted fluoromethane and fluoroethene as C–F donors and concluded that the average F···H distance of the C(sp^3)–F···H–O, C(sp^2)–F···H–O hydrogen bond is 1.9 Å using ab initio calculations.[13] They also found that examples of C–F···H–O and C–F···H–N hydrogen bonds are rare in the Cambridge Structural Database System (CSDS) and showed that the F···H–X angles are dispersed (the statistically found C–F···H–O angles are not within the certainty range). Therefore, they concluded that the interaction is weak. On the other hand, Caminati et al. observed the free jet millimeter wave spectra of the CH_2F_2···H_2O system, and concluded that the optimized distance r(F···H) = 2.20 Å and the angles ∠(F···H–O) and ∠(C–F···H) are 135 and 93°, respectively.[14]

Our studies of the C–F···M$^+$ interaction revealed that the C–F unit attracts all kinds of cations by a cation–dipole interaction as the main driving force.[15] Therefore, we can deduce that C–F can be a proton acceptor because the interaction also operates in the polarized $X^{\delta-}$–$H^{\delta+}$ (X = O, N) system.

Based on this speculation, we employed the cyclophane skeleton for investigating the C–F···H–O hydrogen bond. Phenol and fluorobenzene units in cyclophane **1** are fixed and close to each other (Figure 1). Its spectral features can be compared to those of the structurally analogous cyclophanes **2** and **3**. The C–F···H–O distance (ca. 1.9 Å) and C–F···H and F···H–O angles (ca. 99.5 and 156°) of **1** were estimated using simple molecular-model considerations. These values are close to those estimated by Howard et al. and Caminati et al. Therefore, cyclophane is thought to be an appropriate system for the observation of the C–F···H–O hydrogen bond. In this report, synthesis of the

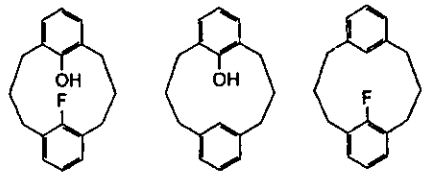

1 **2** **3**

Figure 1. Structures of cyclophanes **1**–**3**

[a] Department of Chemistry, Faculty of Science, Kyushu University,
Ropponmatsu 4-2-1, Chuo-ku, Fukuoka 810-8560, Japan
Fax: (internat.) + 81-92-726-4755
E-mail: takemura@chem.rc.kyushu-u.ac.jp
[b] Department of Chemistry, Faculty of Science, Kyushu University,
Hakozaki 6-10-1, Higashi-ku, Fukuoka 812-8581, Japan
[c] Institute for Materials Chemistry and Engineering, Kyushu University,
Hakozaki 6-10-1, Higashi-ku, Fukuoka 812-8581, Japan
[‡] Present address: Department of Applied Chemistry, Faculty of Engineering, Saitama University,
255 Shimo-ohkubo, Sakuraku, Saitama 338-8570, Japan
Supporting information for this article is available on the WWW under http://www.eurjoc.org or from the author.

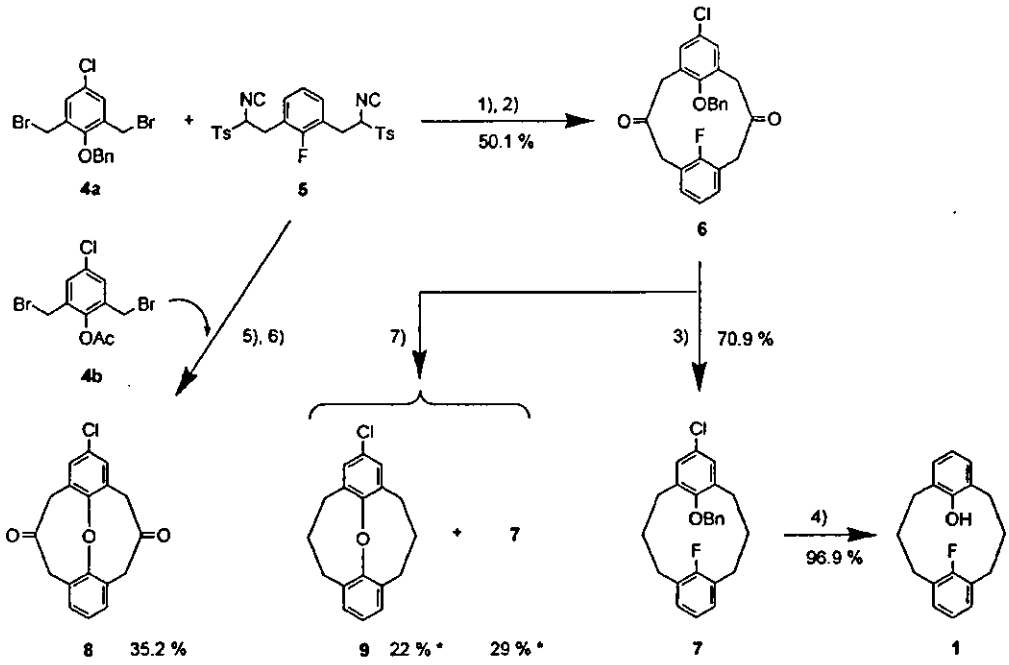

Scheme 1. Synthetic strategies of the cyclophane **1**: 1) Bu_4NI, CH_2Cl_2/aq. NaOH; 2) concd. HCl; 3) Zn/HCl (g), diethyl ether; 4) 10% Pd/C, $HCOONH_4$, MeOH; 5) NaH, DMF; 6) concd. HCl; 7) $NH_2NH_2{\cdot}H_2O$, KOH, diethylene glycol: * each yield was calculated based on the integration of signals in ^1H NMR spectrum

cyclophane, structural analysis and spectral features are discussed as one approach for investigating the C−F···H−O hydrogen bond.

Results and Discussion

Synthesis

The [3.3]metacyclophane skeleton was constracted by the TosMIC method (Scheme 1).[16] However, an unexpected ether product **8** was obtained by the initially chosen strategies employing a cyclization reaction between the acetyl-protected dibromide **4b** and TosMIC derivative **5** in DMF with NaH as the base at room temperature. This disadvantage was overcome by altering the protecting group from an acetyl to a benzyl group. The phase-transfer reaction between **4a** and **5** followed by treatment of the reaction mixture with aq. HCl afforded the diketone **6** in 50.1% yield. The Wolff−Kischner reduction of the cyclophane diketone **6** gave **7** and an ether product **9**, but the separation of each product from the mixture was difficult. Therefore, compound **6** was reduced by the modified Clemmensen reduction procedure,[17] which gave **7** in 70.9% yield. Deprotection and dechlorination were simultaneously achieved by treating compound **7** with 10% Pd/C in the presence of ammonium formate. Cyclophane **1** was thus obtained in good yield from **7** (96.9%). The analogous reference compounds **2** and **3** were synthesized using the literature method reported by Osada et al.[18]

Crystallographic Analysis

Crystallographic analysis of **1** at low temperature (123 K) revealed that two kinds of molecules exist in the crystal. One of them has an O−H proton almost parallel to the benzene ring, which was observed in 80% probability. An O−H of another molecule is twisted and the proton is near the F atom. In Figure 2, these protons are shown in one molecule. The dihedral angles are ∠C(17)−C(18)−O(1)−H(19) = 1.7° and ∠C(17)−C(18)−O(1)−H(20) = 51.3°. The F···H(20) distance is 2.11 Å, which is much shorter than the sum of the van der Waals radii (2.67 Å) of the H atom (1.20 Å) and F atom (1.47 Å).[19] On the other hand, the F···H(19) distance is 2.90 Å and thus, H(19) apparently has no interaction with the F atom. The observed angles, ∠C(9)−F···H(20) = 105.5° and O−H(20)···F = 131.6°, and the F···H(20) distance are fairly near the values reported by Howard et al. and Caminati et al. The former found the potential minimum of the C(sp^2)−F···H−O hydrogen bond at 1.9 Å and the latter observed the angles and distances of ∠C−F···H−O = 93°, ∠O−H···F = 135° and r = 2.20 Å in the CH_2F_2−H_2O system. Furthermore, the O−H(20) distance is 0.99 Å, while O−H(19) is 0.82 Å. The two facts, formerly described as the short F···H(20) distance and the elongated O−H(20) bond, apparently indicate the existence of a hydrogen bond between H(20) and the F atom. However, the proportion of the hydrogen-bonded H atom is only 20%, and it is thus a weak interaction. According to the Boltzmann distribution law, the energy difference between O(19)−H and O(20)−H is only 1.6 kJ mol^{-1}, which can roughly be considered as the stabilization energy of the C−F···HO hydrogen bond of this system at 123 K.

Spectroscopic Investigations

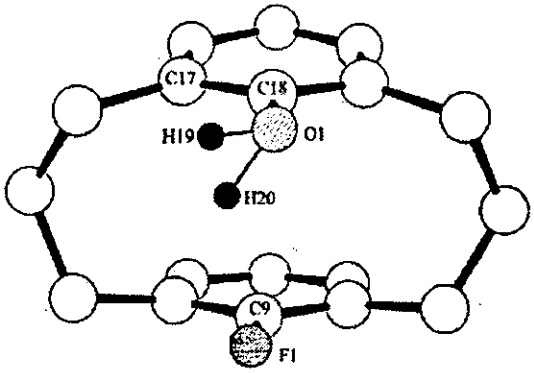

Figure 2. Molecular structure of the cyclophane 1

IR Spectra

In the IR spectra (Table 1), the ν_{OH} bands of **1** and **2** appeared as a sharp band around 3620 cm^{-1} in methylcyclohexane and CCl_4 at the concentration of 1.0×10^{-1} mol dm^{-3}. However, in diluted solution (10^{-2}, 10^{-3} and 10^{-4} mol dm^{-3}), no substantial changes were observed.

Table 1. IR spectra (ν_{OH} in cm^{-1}) of **1** and **2**: (A) crystal (transmittance IR), (B) KBr pellet, (C) in methylcyclohexane (1.0×10^{-4} mol dm^{-3}), and (D) in CCl_4 (1.0×10^{-4} mol dm^{-3})

	1	**2**
(A)	3610, 3560	3541, 3471
(B)	3610, 3560	3542, 3473
(C)	3620	3618
(D)	3621	3621

As seen in the crystallographic analysis, 20% of the OH proton binds to the F atom of **1**. Therefore, the IR spectra of the crystalline state are essential to detect the hydrogen bond. In the crystal lattice, the OH group is independent and no intermolecular interaction was observed (see Supporting Information; footnote on the first page of this article). Therefore, the band in the transmittance spectra of **1** should show the bands of the hydrogen-bond-free O–H and the C–F···H–O band. The transmittance IR spectra of the crystals of **1** and **2** were almost identical to those measured in KBr pellets. Both cyclophanes **1** and **2** have two ν_{OH} bands. In the case of **1**, a relatively broad band appears at 3560 cm^{-1} accompanied by a sharp band at 3610 cm^{-1}. Similarly, compound **2** has a relatively broad band at 3471 cm^{-1} and a sharp band at 3541 cm^{-1}. Unfortunately, crystallographic analysis of compound **2** failed, so the molecular arrangement and information about the hydrogen-bond pattern in the crystal are unknown.[20] Further discussion seems to be difficult because assignment of those ν_{OH} bands cannot be achieved. However, we can speculate that the C–F···H–O hydrogen bond may have anti-hydrogen-bond character because both bands of **1** are blue-shifted (70–90 cm^{-1}) compared to those of **2**.[21] The $\Delta\nu_{OH}$ is equivalent to the C–F···H–O hydrogen bond energy of 0.84–1.1 kJ·mol^{-1}.

NMR Spectra

Because the IR spectra in solution did not give any information, the ^1H and ^{19}F NMR spectra were evaluated. These results are summarized in Table 2. The chemical shifts of the phenolic OH protons of **1** and **2** in $CDCl_3$ at the concentrations of 1.0×10^{-1}, 1.0×10^{-2} and 1.0×10^{-3} mol·dm^{-3} were the same within the experimental errors [$\delta_{OH}(1) = 4.87$ ppm; $\delta_{OH}(2) = 4.61$ ppm]. On the other hand, the OH proton of **1** in [D_{14}]methylcyclohexane showed concentration-dependent chemical shifts, i.e., the OH proton signal appeared at $\delta = 4.75$ ppm (1.0×10^{-1} mol·dm^{-3}), 4.62 ppm (1.0×10^{-2} mol·dm^{-3}), and 4.60 ppm (1.0×10^{-3} mol·dm^{-3}). In the case of cyclophane **2**, such chemical shifts were not observed at a concentration of 1.0×10^{-1} to 1.0×10^{-3} mol·dm^{-3}; it appears at $\delta = 4.20$ ppm as a singlet. Although an interaction with $CDCl_3$ is apparent, the OH signal of **1** appears at a lower field than that of **2**, and this is the same in the noninteracting solvent, [D_{14}]methylcyclohexane. Therefore, the C–F···H–O hydrogen bond is obvious in the ^1H NMR spectra. Moreover, specific phenomena were seen in the spectrum of **1**, viz., the OH signal appeared as a doublet ($J_{H,F} = 6.0$ Hz) which shows the through-space coupling with the fluorine atom. By irradiation of the F atom, the coupling disappeared and the doublet became a singlet. Furthermore, in a donating solvent such as [D_6]DMSO, the signal appeared as a singlet. This is further evidence of an O-H···F interaction.

The δ_F values of cyclophanes **1** and **3** were compared in their ^{19}F NMR spectra (Table 2). The differences were small, but in both $CDCl_3$ and [D_{14}]methylcyclohexane, chemical shifts of the F signal of cyclophane **1** are higher than those of **3** (1.0–1.6 ppm). This high-field shift of the F signal reminds us of similar phenomena in the metal complexes of fluorinated cage compounds.[22] The C–F···M^+ attractive interaction has now been unambiguously established by this group and Plenio et al.,[23,24] and the high-field shift of the F signal usually occurs during the C–F···M^+ interaction. Therefore, in the C–F···$H^{\delta+}$–$O^{\delta-}$ system, the same phenomena should also be observed. Here, again, the hydrogen bond is confirmed by comparison of the ^{19}F NMR spectra of cyclophanes **1** and **3**.

The temperature-dependent shift of the OH proton is another interesting feature in the study of the hydrogen bond. Variable-temperature ^1H NMR spectra of **1** and **2** were measured in nonpolar and polar solvents, [D_{14}]methylcyclohexane and [D_6]DMSO. As shown in Figure 3, the OH proton spectra of **1** and **2** are strongly temperature-dependent, especially below 240 K. In the case of **2**, two kinds of OH proton signals appeared below 243 K. At this temperature, conformational changes of the trimethylene bridge (boat ⇄ chair) are involved.[25] Therefore, the two OH protons correspond to those of the conformational isomers. In the case of cyclophane **1**, conformational changes also occur below 243 K. However, only one kind of OH proton

Table 2. NMR shifts of OH and F signals (1.0×10^{-2} mol·dm^{-3}) of the cyclophanes at 25 °C (A) in [D_{14}]methylcyclohexane, and (B) in $CDCl_3$

	^{1}H, δ(OH)		^{19}F, δ(^{19}F)	
	(A)	(B)	(A)	(B)
1	4.60 [d, J(H−F) = 6.6 Hz]	4.86 [d, J(H−F) = 6.0 Hz]	−120.3 (br. s)	−119.9 (br. s)
2	4.21 (s)	4.58 (br. s)	−	−
3	−	−	−118.7 (s)	−118.9 [d, J(H−F) = 3.5 Hz]

was observed. In the polar solvent ([D_6]DMSO), the OH signal of **1** is shifted to a high-field region compared to that of **2** (Δδ = −0.25 ppm at 298 K). This phenomenon reflects that the hydrogen bond between **1** and DMSO is inhibited by the intramolecular hydrogen bond.

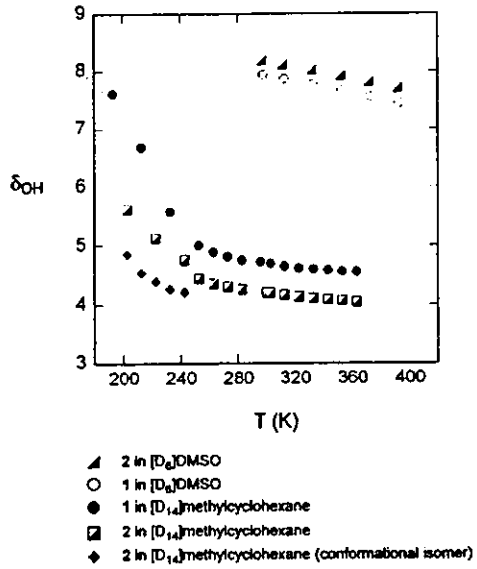

Figure 3. Plots of δ_{OH} in [D_6]DMSO and [D_{14}]methylcyclohexane at various temperatures

The difference of chemical shift of the OH proton, Δδ, between **1** and **2** is almost constant (Δδ ≈ 0.5 ppm in [D_{14}]methylcyclohexane) between 273 and 363 K, and the Δδ value indicates the C-F···H−O binding energy. Schaefer represented the relationship between hydrogen-bond energy and chemical shift of *ortho*-substituted phenols.[26] The empirical equation $\Delta\delta_{OH} = -0.4 + E$ (E is the hydrogen-bond energy in kcal·mol^{-1}) can be applied to our cyclophane system. According to the equation, the C-F···H−O hydrogen bond of **1** is estimated to be 0.89 kcal·mol^{-1} (3.7 kJ mol^{-1}) in [D_{14}]methylcyclohexaneand 0.65 kcal·mol^{-1} (2.7 kJ·mol^{-1}) in [D_6]DMSO at 298 K.

From the results of the crystallographic analysis, IR spectra and NMR spectra, we estimated the C-F···H−O hydrogen bond energy of **1** to be 0.84−1.6 kJ·mol^{-1} in the solid state and 2.7−3.7 kJ·mol^{-1} in solution.

Conclusion

A [3.3]metacyclophane, which is composed of a phenol unit and a fluorobenzene unit, was synthesized. It is a simple model for the investigation of the C−F···H−O hydrogen bond. The cyclophane skeleton is suitable for realizing the ideal F···H−O distance and angles, and to obtain the entropy. Actually, evidence for the C−F···H−O hydrogen bond is observed from the results of the crystallographic analysis. Two kinds of OH hydrogen atoms are observed and one of them is pointing towards the fluorine atom. The H···F distance is shorter than the sum of the van der Waals radii of the H and F atoms, and the O−H bond is longer than that of another proton which is separated from the F atom. In the ^{1}H NMR spectrum, the OH proton signal of **1** appears at a lower field than that of the fluorine-free analog **2**. Furthermore, through-space coupling between the F atom and OH proton is observed. Although the IR spectra did not give a clear result, it is speculated that the C−F···H−O hydrogen bond has an anti-hydrogen-bond character. The C−F···H−O hydrogen bond energy in this system was estimated to be 0.84−3.7 kJ·mol^{-1} according to the results of the crystallographic analysis and the IR and NMR spectra. Although the C−F···H−O hydrogen bond is very rare in the crystallographic database, it is possible to observe it by this simple molecular design. A forcibly approached OH and CF unit with the appropriate distance and angle clarified this weak interaction.

Experimental Section

General Procedure: Melting points (uncorrected): Yanaco MP-500D apparatus in Ar sealed tubes. NMR: Bruker DPX-400 (400.1 MHz for ^{1}H, 100.6 MHz for ^{13}C, and 376.5 MHz for ^{19}F with TMS and $CFCl_3$ as internal references, respectively) and JEOL GSX 270 (270 MHz for ^{1}H and 67.9 MHz for ^{13}C). IR: JASCO IR-700 [methylcyclohexane in NaCl cells (0.1 and 0.5 mm) at 25°C]. FAB and EI MS: JEOL JMS-SX/SX102A. Elemental analysis: the Service Centre of the Elementary Analysis of Organic Compounds affiliated with the Faculty of Science, Kyushu University.

Crystallographic Data of 1: $C_{18}H_{19}OF$, M_r = 270.35 g·mol^{-1}, platelet crystal (grown from *n*-hexane), size 0.40 × 0.20 × 0.05 mm, monoclinic, space group $P2_1$ (no. 4), a = 8.719(1) Å, b = 8.552(1) Å, c = 9.599(1) Å, V = 695.3(2) Å^3, Z = 2, $\rho_{calcd.}$ = 1.291 g·cm^{-3}, μ(Cu-K$_\alpha$) = 7.01 cm^{-1}, F(000) = 288.00, T = −150 ± 1 °C using the ω-2θ scan technique to a maximum 2θ value of 136.4°. A total

of 4177 reflections were collected. The final cycle of the full-matrix least-squares refinement was based on 1990 observed reflections [$I > 2\sigma(I)$] and 182 variable parameters and converged with unweighted and weighted agreement factors of $R = 0.067$, $Rw = 0.202$, and GOF = 1.09. The maximum and minimum peaks on the final difference Fourier map corresponded to 0.22 and −0.25 $e^{-}\cdot Å^{-3}$, respectively. The ratio of two kinds of molecules in the crystal was calculated and the probability of 0.8:0.2 afforded the optimal result. CCDC-213846 contains the supplementary crystallographic data for this paper. These data can be obtained free of charge at www.ccdc.cam.ac.uk/conts/retrieving.html [or from the Cambridge Crystallographic Data Centre, 12 Union Road, Cambridge CB2 1EZ, UK; Fax: (internat.) + 44-1223/336-033; E-mail: deposit@ccdc.cam.ac.uk].

1-Benzyloxy-4-chloro-2,6-bis(hydroxymethyl)benzene: The compound was prepared by the reaction between 4-chloro-2,6-bis(hydroxymethyl)phenol and benzyl bromide with K_2CO_3 as a base in acetone (86.4%). Recrystallization from toluene/methanol gave a colorless powder; m.p. 125.2−126.9 °C. ^{1}H NMR ([D$_6$]DMSO): δ = 7.46−7.35 (m, 5 H, ArH), 7.33 (s, 2 H, ArH), 5.27 (t, $^3J_{H,H}$ = 5.5 Hz, 2 H, OH), 4.83 (s, 2 H, CH_2), 4.52 (d, $^3J_{H,H}$ = 6.0 Hz, 4 H, CH_2) ppm. FAB-MS: *m/z* = 278.1, 280.1. $C_{15}H_{15}ClO_3$ (278.73): calcd. C 64.64, H 5.42; found C 64.72; H 5.46.

1-Benzyloxy-2,6-bis(bromomethyl)-4-chlorobenzene (4a): The compound was prepared by treatment of 1-benzyloxy-4-chloro-2,6-bis(hydroxymethyl)benzene with PBr_3 in diethyl ether (yield 86.8%). The resultant powder was recrystallized from *n*-hexane. Colorless solid, m.p. 97.3−98.5 °C. ^{1}H NMR ($CDCl_3$): δ = 7.53−7.39 (m, 5 H, ArH), 7.38 (s, 2 H, ArH), 5.16 (s, 2 H, CH_2), 4.46 (s, 4 H, CH_2) ppm. FAB-MS: *m/z* = 402.9, 403.9, 404.9 [M + H$^+$]. $C_{15}H_{13}Br_2ClO\cdot 1/12C_6H_{14}$ (411.71): calcd. C 45.22, H 3.47; found C 45.08; H 3.30.

1-Fluoro-2,6-bis[2-isocyano-2-(4-tolylsulfonyl)ethyl]benzene (5): The compound was synthesized by reaction between 2,6-bis(bromomethyl)-1-fluorobenzene and TosMIC (yield 62.8%) according to the literature method.[16] Recrystallization from CH_2Cl_2/diethyl ether gave colorless fine crystals, m.p. 112 °C (dec.). ^{1}H NMR ($CDCl_3$): δ = 7.91, 7.45 (AB q, $^3J_{H,H}$ = 8.4 Hz, 8 H, ArH), 7.28−7.13 (m, 3 H, ArH), 4.68 (dd, $^3J_{H,H}$ = 10.8 Hz, 2 H, CH), 3.73−3.04 (m, 4 H, CH_2), 2.50 (s, 6 H, CH_3) ppm. FAB-MS: no molecular peak was found. $C_{26}H_{23}FN_2S_2O_4$ (510.60): calcd. C 61.16, H 4.54, N 5.49; found C 60.88, H 4.63; N 5.52.

9-Benzyloxy-6-chloro-18-fluoro[3.3]metacyclophane-2,11-dione (6): A mixture of CH_2Cl_2 (1.3 L), 40% aq. NaOH (50 mL), and nBu_4NI (1.69 g, 4.58 mmol) was heated under reflux with vigorous stirring. To this mixture, a solution of **4a** (4.05 g, 10.0 mmol) and **5** (5.62 g, 11.0 mmol) in CH_2Cl_2 (250 mL) was added dropwise over a period of 6 h. Additional heating and stirring were continued for 5 h. After cooling, the organic phase was separated and washed with brine. The solution was concentrated to ca. 300 mL, conc. HCl (30 mL) was added and the mixture was stirred at room temperature for 40 min. The organic phase was separated, washed with water and dried with $MgSO_4$. The solvent was removed under reduced pressure and a small amount of acetone was added. After several hours, the precipitated colorless prisms were collected (yield 2.12 g, 50.1%), m.p. 138.4−138.8 °C. ^{1}H NMR ($CDCl_3$): δ = 7.53−7.32 (m, 3 H, ArH), 7.24 (s, 2 H, ArH), 7.12 (dd, $^3J_{H,H}$ = 7.0 Hz, 2 H, ArH), 7.05−7.03 (m, 2 H, ArH), 6.84 (t, $^3J_{H,H}$ = 7.5 Hz, 1 H, ArH), 4.32 (s, 2 H, CH_2), 3.80−3.15 (m, 8 H, CH_2) ppm. FAB-MS: *m/z* = 423 [M + H$^+$]. $C_{25}H_{20}ClFO_3$ (422.88): calcd. C 71.01, H 4.77; found C 71.03; H 4.78.

9-Benzyloxy-6-chloro-18-fluoro[3.3]metacyclophane (7): Dry HCl gas was bubbled into dry ether (80 mL) at −10 °C for 1 h, and compound **6** (1.48 g, 3.5 mmol) was added. The resultant suspension was cooled to −20 °C and activated Zn powder (2.0 g) was added in small portions. After the addition, the temperature was raised to −5 °C and the mixture stirred for 2 h. The resultant mixture was poured onto crushed ice (40 g) and the organic phase was separated. The aqueous phase was extracted twice with ether, and all the diethyl ether solutions were combined. They were washed with aq. $NaHCO_3$ and dried with $MgSO_4$, the solvent was removed and the resultant powder was recrystallized from *n*-hexane. Colorless prisms (yield 980 mg, 70.9%), m.p. 102.1−102.6 °C. ^{1}H NMR ($CDCl_3$): δ = 7.53−7.31 (m, 5 H, ArH), 6.73 (m, 1 H, ArH), 6.63 (dd, $^3J_{H,H}$ = 7.0 Hz, 2 H, ArH), 6.52 (s, 2 H, ArH), 4.65 (s, 2 H, CH_2), 3.10−3.02 (m, 4 H, CH_2), 2.52−2.33 (m, 6 H, CH_2), 1.85−1.75 (m, 2 H, CH_2) ppm. FAB-MS: *m/z* = 394 [M$^+$]. $C_{25}H_{24}ClFO$ (394.91): calcd. C 76.03, H 6.13; found C 75.99, H 6.10.

18-Fluoro-9-hydroxy[3.3]metacyclophane (1): A mixture of the cyclophane **7** (197 mg, 0.50 mmol) and ammonium formate (221 mg, 3.5 mmol) in MeOH (60 mL) was stirred at room temperature under N_2; 10% Pd/C (100 mg) was added to the mixture, which was then stirred at room temperature for 5 h. The mixture was filtered through Celite and the solvent was removed. The resultant mixture was extracted with diethyl ether and the solution was washed with brine and dried with $MgSO_4$. After removal of the solvent, compound **1a** was obtained as a white powder, which was recrystallized from *n*-hexane. Colorless prisms (yield 131 mg, 96.9%), m.p. 84.5−84.8 °C. ^{1}H NMR ($CDCl_3$): δ = 6.63−6.53 (m, 5 H, ArH), 6.39 (t, $^3J_{H,H}$ = 7.0 Hz, 1 H, ArH), 4.87 (d, $^3J_{H,H}$ = 6.0 Hz, 1 H, CH_2), 3.09−2.99 (m, 4 H, CH_2), 2.65−2.54 (m, 4 H, CH_2), 2.42−2.35 (m, 2 H, CH_2), 1.92−1.81(m, 2 H, CH_2) ppm. FAB-MS: *m/z* = 270 [M$^+$]. $C_{18}H_{19}FO$ (270.34): calcd. C 79.97, H 7.08; found C 79.91, H 7.08.

1-Acetoxy-2,6-bis(bromomethyl)-4-chlorobenzene (4b): A mixture of 2,6-bis(bromomethyl)-4-chlorophenol (6.29 g, 20 mmol), acetic anhydride (2.4 mL, 25 mmol), and $BF_3\cdot Et_2O$ (0.1 mL, 0.8 mmol) in dry diethyl ether (20 mL) was stirred at room temperature for 10 h. The mixture was added to water (20 mL) and the resultant white powder was collected by filtration and washed with water to give the pure compound (yield 6.10 g, 85.6%). Recrystallization from *n*-hexane gave colorless needles, m.p. 143.3−144.2 °C. ^{1}H NMR ($CDCl_3$): δ = 7.39 (s, 2 H, ArH), 4.31(s, 4 H, CH_2), 2.15 (s, 3 H, CH_3) ppm. FAB-MS: *m/z* = 354.9, 356.9, 358.9 [M + H$^+$]. $C_{10}H_9Br_2ClO_2$ (356.44): calcd. C 33.70, H 2.55; found C 33.80, H 2.50.

Compound 8: A solution of **4b** (3.56 g, 10 mmol) and **5** (5.11 g, 10 mmol) in dry DMF (500 mL) was added to a stirred mixture of NaH (60% in mineral oil, 1.20 g, 30 mmol) and dry DMF (700 mL) at room temperature over a period of 10 h. Additional stirring was continued for 10 h and then the mixture was quenched with MeOH. The solvent was removed under reduced pressure and MeOH was added. After several hours, pale-yellow crystals precipitated. The crystals were collected by filtration and dissolved in CH_2Cl_2 (300 mL). Concentrated HCl (20 mL) was added to the solution, which was stirred at room temperature for 30 min. The organic phase was separated, washed with water and dried with $MgSO_4$. The solvent was removed and a small amount of acetone was added to the residue. Colorless prisms that precipitated after several hours were collected (yield 1.10 g, 35.2%), m.p. 259.7−260.1 °C. ^{1}H NMR ($CDCl_3$): δ = 7.17−7.13 (m, 5 H, ArH), 3.72−3.56

(m, 8 H, CH_2) ppm. FAB-MS: *m/z* = 313 [M + H^+]. $C_{18}H_{13}ClO_3$ (312.75): calcd. C 69.13, H 4.19; found C 69.15, H 4.20.

Compound 9: A mixture of **8** (665 mg, 2.13 mmol), 80% hydrazine hydrate (3.4 mL, 53 mmol), diethylene glycol (30 mL), and KOH (1.57 g, 23.8 mmol) was heated at 120 °C for 2 h, and then the temperature was raised to 180 °C. The water generated during the reaction was removed by a Dean–Stark condenser. Additional heating was continued for 2 h, then the mixture was cooled, poured into water and extracted twice with CH_2Cl_2. The organic phase was washed with water and brine, then dried with $MgSO_4$. The solvent was removed and the residue was recrystallized from MeOH. Colorless needles (421 mg, 69.4%). M.p. 112.3–112.7 °C. ^1H NMR ($CDCl_3$): δ = 6.97–6.89 (m, 5 H, ArH), 3.21–3.13 (m, 2 H, CH_2), 2.81–2.70 (m, 2 H, CH_2), 2.39–2.32 (m, 1 H, CH_2), 1.76–1.55 (m, 1 H, CH_2) ppm. FAB-MS: *m/z* = 284 [M^+]. $C_{18}H_{17}ClO$ (284.78): calcd. C 75.92, H 6.02; found C 75.84, H 6.05.

[1] P. Murray-Rust, W. C. Stallings, C. T. Monti, R. K. Prestone, J. P. Glusker, *J. Am. Chem. Soc.* **1983**, *105*, 3206–3214.
[2] J. D. Dunitz, R. Taylor, *Chem. Eur. J.* **1997**, *3*, 89–98.
[3] L. Shimoni, J. P. Glusker, *Struct. Chem.* **1994**, *5*, 383–397.
[4] S. J. Borwick, J. A. K. Howard, C. W. Lehmann, D. O'Hagan, *Acta Crystallogr., Sect. C* **1997**, *53*, 124–126.
[5] T. J. Barbarich, C. D. Rithner, S. M. Miller, O. P. Anderson, S. H. Strauss, *J. Am. Chem. Soc.* **1999**, *121*, 4280–4281.
[6] M. Pham, M. Gdaniec, T. Polonski, *J. Org. Chem.* **1998**, *63*, 3731–3734.
[7] N. Shibata, B. K. Das, K. Harada, Y. Takeuchi, M. Bando, *Synlett* **2001**, 1755–1758.
[8] K.-M. Marstokk, H. MØllendal, *Acta Chem. Scand.* **1999**, *53*, 202–208.
[9] A. Fujii, A. Iwasaki, N. Mikami, *Chem. Lett.* **1997**, 1099–1100.
[10] A. Kovács, I. Mascsári, I. Hargittai, *J. Phys. Chem. A* **1999**, *113*, 3110–3114.
[11] A. D. Headley, S. D. Starnes, *J. Comput. Chem.* **2000**, *21*, 426–431.
[12] J. E. Monat, R. R. Toczyowski, S. M. Cybulski, *J. Phys. Chem. A* **2001**, *105*, 9004–9013.
[13] J. A. K. Howard, V. J. Hoy, D. O'Hagan, G. T. Smith, *Tetrahedron* **1996**, *52*, 12613–12622.
[14] W. Caminati, S. Melandri, I. Rossi, P. G. Favero, *J. Am. Chem. Soc.* **1999**, *121*, 10098–10101.
[15] H. Takemura, S. Nakashima, N. Kon, M. Yasutake, T. Shinmyozu, T. Inazu, *J. Am. Chem. Soc.* **2001**, *123*, 9293–9298.
[16] [16a] K. Kurosawa, M. Suenaga, T. Inazu, T. Yoshino, *Tetrahedron Lett.* **1982**, *23*, 5335–5338. [16b] T. Shinmyozu, Y. Hirai, T. Inazu, *J. Org. Chem.* **1986**, *51*, 1551–1555.
[17] S. Yamamura, M. Toda, Y. Hirata, *Org. Synth. Coll. Vol.* **1988**, *6*, 289–292.
[18] [18a] S. Osada, M. Suenaga, Y. Miyahara, T. Shinmyozu, T. Inazu, *Mem. Fac. Sci., Kyushu Univ., Ser. C* **1993**, *19*, 33–38. [18b] S. Osada, Y. Miyahara, N. Shimizu, T. Inazu, *Chem. Lett.* **1995**, 1103–1104. [18c] S. Osada, Thesis, Kyushu University, **1995**.
[19] A. Bondi, *J. Phys. Chem.* **1964**, *68*, 441–451.
[20] Crystallographic analysis of *p*-Cl analog of **2** (6-chloro-9-hydroxy[3.3]metacyclophane) succeeded. It showed intermolecular O–H···O hydrogen bonds and even intermolecular Cl···H–O hydrogen bonds. Unpublished results.
[21] [21a] P. Hobza, V. Spirko, H. L. Selzle, E. W. Schlag, *J. Phys. Chem. A* **1998**, *102*, 2501–2504. [21b] E. Cubero, M. Orozco, P. Hobza, F. J. Luque, *J. Phys. Chem. A* **1999**, *103*, 6394–6401. [21c] E. Cubero, M. Orozco, F. J. Luque, *Chem. Phys. Lett.* **1999**, *310*, 445–450. [21d] P. Hobza, Z. Havlas, *Chem. Phys. Lett.* **1999**, *303*, 447–452. [21e] P. Hobza, Z. Havlas, *Chem. Rev.* **2000**, *100*, 4253–4264. [21f] B. J. van der Veken, W. A. Herrebout, R. Szostak, D. N. Shchepkin, Z. Havlas, P. Hobza, *J. Am. Chem. Soc.* **2001**, *123*, 12290–12293.
[22] [22a] H. Takemura, H. Kariyazono, M. Yasutake, N. Kon, K. Tani, K. Sako, T. Shinmyozu, T. Inazu, *Eur. J. Org. Chem.* **2000**, 141–148. [22b] H. Takemura, S. Nakashima, N. Kon, T. Inazu, *Tetrahedron Lett.* **2000**, *41*, 6105–6109. [22c] H. Takemura, *J. Syn. Org. Chem. Jpn.* **2002**, *60*, 963–973.
[23] [23a] H. Takemura, N. Kon, M. Yasutake, H. Kariyazono, T. Shinmyozu, T. Inazu, *Angew. Chem.* **1999**, *111*, 1012–1014; *Angew. Chem. Int. Ed.* **1999**, *38*, 959–961. [23b] H. Takemura, N. Kon, M. Yasutake, S. Nakashima, T. Shinmyozu, T. Inazu, *Chem. Eur. J.* **2000**, *6*, 2334–2337. [23c] H. Takemura, N. Kon, M. Kotoku, S. Nakashima, K. Otsuka, M. Yasutake, T. Shinmyozu, T. Inazu, *J. Org. Chem.* **2001**, *66*, 2778–2783. [23d] H. Takemura, S. Nakashima, N. Kon, M. Yasutake, T. Shinmyozu, T. Inazu, *J. Am. Chem. Soc.* **2001**, *123*, 9293–9298. [23e] H. Takemura, in *Cyclophane Chemistry for the 21st Century* (Ed.: H. Takemura), Transworld Research Network, India, **2003**, p. 127–148.
[24] [24a] H. Plenio, R. Diodone, *Angew. Chem.* **1994**, *106*, 2267–2269; *Angew. Chem. Int. Ed. Engl.* **1994**, *33*, 2175–2177. [24b] H. Plenio, D. Burth, *J. Chem. Soc., Chem. Commun.* **1994**, 2297–2298. [24c] H. Plenio, R. Diodone, *J. Am. Chem. Soc.* **1996**, *118*, 356–367. [24d] H. Plenio, R. Diodone, *Chem. Ber.* **1996**, *129*, 1211–1217. [24e] H. Plenio, R. Diodone, *Chem. Ber./Recueil* **1997**, *130*, 963–968. [24f] H. Plenio, J. Hermann, R. Diodone, *Inorg. Chem.* **1997**, *36*, 5722–5729. [24g] H. Plenio, R. Diodone, D. Badura, *Angew. Chem.* **1997**, *109*, 130–132; *Angew. Chem. Int. Ed. Engl.* **1997**, *36*, 156–158. [24h] H. Plenio, *Chem. Rev.* **1997**, *97*, 3363–3384, and references cited therein.
[25] [25a] H. Takemura, H. Kariyazono, N. Kon, T. Shinmyozu, T. Inazu, *J. Org. Chem.* **1999**, *64*, 9077–9079.. [25b] K. Sako, T. Hirakawa, N. Fujimoto, T. Shinmyozu, T. Inazu, H. Horimoto, *Tetrahedron Lett.* **1988**, *29*, 6275–6278. [25c] K. Sako, T. Shinmyozu, H. Takemura, M. Suenaga, T. Inazu, *J. Org. Chem.* **1992**, *57*, 6536–6541. [25d] M. F. Semmelhack, J. J. Harrison, D. C. Young, A. Gutiérrez, S. Rafii, J. Clardy, *J. Am. Chem. Soc.* **1985**, *107*, 7508–7514.
[26] T. Schaefer, *J. Phys. Chem.* **1975**, *79*, 1888–1890.

Received November 1, 2003

Available online at www.sciencedirect.com
SCIENCE DIRECT®
Biomaterials 26 (2005) 37–46
Biomaterials
www.elsevier.com/locate/biomaterials

Mesoscopic spatial designs of nano- and microfiber meshes for tissue-engineering matrix and scaffold based on newly devised multilayering and mixing electrospinning techniques

Satoru Kidoaki, Il Kuen Kwon, Takehisa Matsuda*

Division of Biomedical Engineering, Graduate School of Medicine, Kyushu University, 3-1-1 Maidashi, Higashiku, Fukuoka City, Fukuoka 812-8582, Japan

Received 2 November 2003; accepted 26 January 2004

Abstract

To design a mesoscopically ordered structure of the matrices and scaffolds composed of nano- and microscale fiber meshes for artificial and tissue-engineering devices, two new electrospinning techniques are proposed: multilayering electrospinning and mixing electrospinning. First, the following four kinds of component polymers were individually electrospun to determine the conditions for producing stable nano- and microfibers by optimizing the formulation parameters (solvent and polymer concentration) and operation parameters (voltage, air gap, and flow rate) for each polymer: (a) type I collagen, (b) styrenated gelatin (ST-gelatin), (c) segmented polyurethane (SPU), and (d) poly(ethylene oxide). A trilayered electrospun mesh, in which individual fiber meshes (type I collagen, ST-gelatin, and SPU) were deposited layer by layer, was formed by sequential electrospinning; this was clearly visualized by confocal laser scanning microscopy. The mixed electrospun-fiber mesh composed of SPU and PEO was prepared by simultaneous electrospinning on a stainless-steel mandrel with high-speed rotation and traverse movement. A bilayered tubular construct composed of a thick SPU microfiber mesh as an outer layer and a thin type I collagen nanofiber mesh as an inner layer was fabricated as a prototype scaffold of artificial grafts, and visualized by scanning electron microscopy.

Keywords: Electrospinning; Multilayering; Mixing; Nanofibers; Microfibers

1. Introduction

The structural design of artificial matrices or scaffolds that mimic the supramolecular structure and biological functions of the extracellular matrix (ECM) is a key issue in tissue engineering and the development of artificial organs. In general, in connective tissues, the ECM forms a composite-like structure of proteoglycans and fibrous proteins such as collagens [1]. The collagen fibrous structures are organized into the mesoscopic three-dimensional fiber network composed of nanoscale multifibrils of collagens [2]. Therefore, a significant guideline for designing the artificial ECM or scaffold may be formation of nanoscale building blocks such as nanofibers [3–6] and its appropriate spatial organization on the mesoscopic scale.

From this viewpoint, electrospinning (ELSP) has recently been drawn strong attention in biomedical engineering [7–14], providing a basis for the fabrication of unique matrices and scaffolds for tissue engineering. ELSP is a spinning method that can produce polymer fibers with diameters ranging from several micros to 100 nm or less under a high-voltage electrostatic field operated between a metallic nozzle of a syringe and a metallic collector in air [15,16]. The fibers are typically deposited in the form of a nonwoven fabric onto a target metallic collector through a random deposition process of projected jet of polymer solution, the so-called cone jet or instable jet [17]. The accumulated charges on the polymer solution ejected from the nozzle induce the radial charge repulsion in the electric field, which induces the instable jet. The nanoscale diameter of the produced fibers and the structure of the nonwoven

*Corresponding author. Tel.: +81-92-642-6210; fax: +81-92-642-6212.
E-mail address: matsuda@med.kyushu-u.ac.jp (T. Matsuda).

0142-9612/$ - see front matter © 2004 Elsevier Ltd. All rights reserved.
doi:10.1016/j.biomaterials.2004.01.063

fabric often resemble the above-mentioned supramolecular feature of ECM. If the random deposition process of fibers in the instability jet is appropriately controlled on the mesoscopic scale, the higher-ordered spatial placement of the nano- and microfibers in the ELSP fabrics will be realized. In addition, the high-speed movement of the collector or nozzle may produce oriented meshes and more higher-ordered macroscopic devices. Example is given by compliant vascular scaffold made of SPU meshes, which was pioneered by Annis et al. [18], almost a quarter century ago.

In this study, to materialize this concept, we developed two novel ELSP techniques: multilayering ELSP and (multicomponent) mixing ELSP, both of which are composed of different nano- and microfibers (see Scheme 1). In the multilayering ELSP, after electrospinning the first polymer, the second polymer is sequentially electrospun on the same target collector. Such a sequential spinning process can produce a multilayered fiber mesh, in which a hierarchically ordered structure composed of different kinds of polymer mesh should be obtained. For the mixing ELSP, two different polymers are simultaneously electrospun from different syringes under special conditions. The produced polymer fibers are mixed on the same target collector, resulting in the formation of a mixed fiber mesh.

Examples of fabrications with multilayering and mixing ELSP using four different biopolymers or synthetic polymers such as type I collagen, polymerizable styrenated gelatin (ST-gelatin), segmented polyurethane (SPU), and poly(ethylene oxide) (PEO), were demonstrated. A bilayered tubular construct composed of SPU and type I collagen fibers was fabricated as a prototype of a small-diameter compliant artificial graft. The potential use of these techniques for the preparation of tissue-engineering matrices, scaffolds, and devices is discussed.

2. Materials and methods

2.1. Electrospinning apparatus

A custom-designed electrospinning apparatus was constructed using a high-voltage power supply (HSP-30k-2; Nippon Stabilizer, Inc., Osaka, Japan), an infusion pump (Model 22; Harvard Apparatus Inc., Holliston, MA), a glass syringe, a stainless-steel blunt-ended needle (outer diameter: 1.0 mm, inner diameter: 0.8 mm), and an aluminum plate-type collector (15 × 20 cm) or a custom-made rotating and traversing mandrel-type collector (outer diameter: 3 mm, length: 20 cm; Four Leaves, Inc., Osaka, Japan). The syringe was horizontally fixed on the infusion pump and the sample solution was led through a teflon tube to the needle that was vertically placed at the center of a 15-cm-diameter disk-type electrode and placed above the collector using insulated ceramic poles (Scheme 2). The sample solution was electrostatically drawn from the tip of the needle by applying a high voltage between the disk electrode and the collector. The flow rate of the solution, applied voltage, and distance between the needle tip and collector (air gap) were set between 1.0 and 5.0 ml/h, 7.0 and 30.0 kV, and 5.0 and 30.0 cm, respectively.

2.2. Polymers

The polymers used are: (a) type I collagen from bovine skin (acid soluble, lyophilized powder; Koken

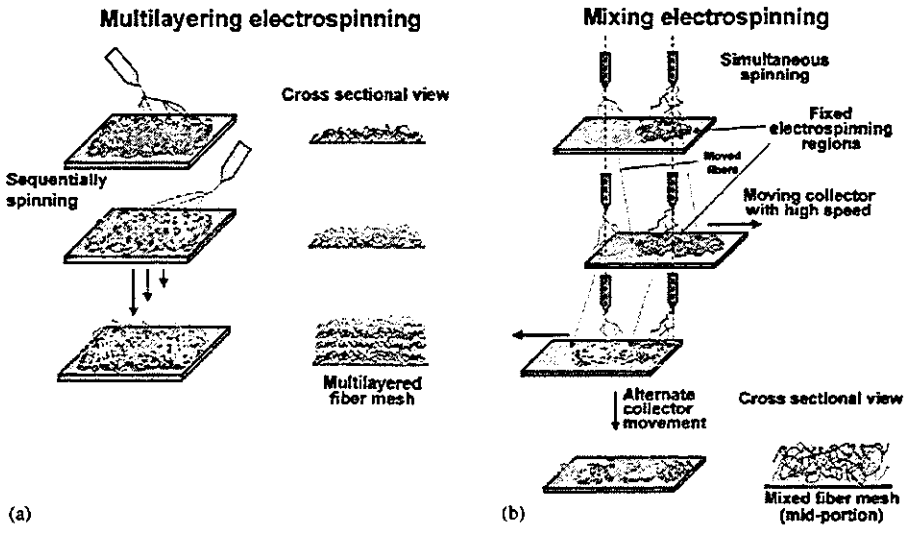

Scheme 1. Proposed electrospinning techniques: (a) multilayering and (b) mixing.

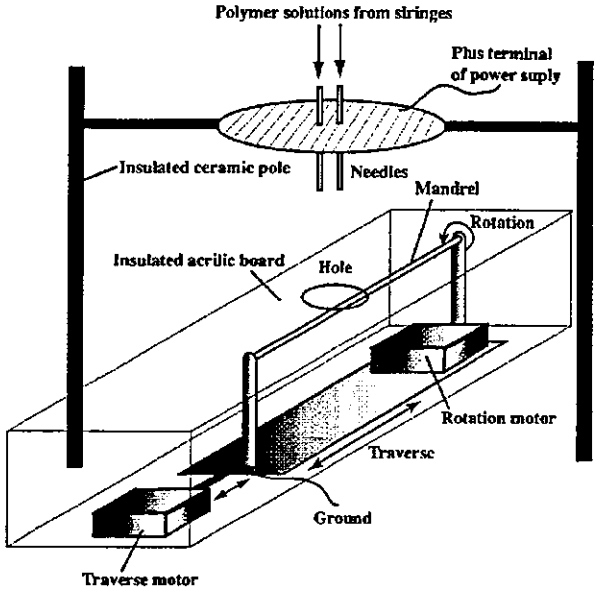

Scheme 2. Apparatus for mixing electrospinning.

Co., Ltd., Tokyo, Japan), (b) ST-gelatin: gelatin molecule (molecular weight: 9.6×10^4 g/mol, total amino group: 36.8 per molecule) derivatized with 33.6 styrene groups on the lysine residues and synthesized according to the method previously reported by us [19,20], (c) SPU (Cardiomat 610, Kontron Instruments Inc., Boston, MA), and (d) PEO, molecular weight: 500,000 (Wako Pure Chemical Ind., Ltd., Osaka, Japan). Type I collagen and ST-gelatin were dissolved in 1,1,1,3,3,3-hexafluoro-2-propanol (HFIP, Sigma Chemical Co., St. Louis, MO) at concentrations between 1.0 and 7.0 wt%, and 1.0 and 10.0 wt%, respectively. SPU was dissolved at 15.0 wt% in tetrahydrofuran (THF, Wako). The PEO solution was prepared at concentrations between 1.0 and 4.5 wt% in chloroform (Wako).

2.3. Photopolymerization

The visible-light-induced photopolymerization of the electrospun ST-gelatin fiber mesh was performed with 1,7,7-trimethyl-bicyclo[2.2.1]heptane-2,3-dione (camphorquinone, Sigma) as a radical generator. Photoirradiation was conducted using a TOKUSO Power Lite (xenon lamp with UV- and IR-cutoff filter: Tokuyama Co., Ltd., Yamaguchi, Japan), and irradiation intensity was measured with a photometer (laser power meter HP-2: Pneum Co., Ltd., Saitama, Japan). Irradiation intensity and time were set at 50 mW/cm^2 and 10 min, respectively.

2.4. Ultraviolet (UV)-light-induced crosslinking

The UV-light-induced crosslinking of the electrospun type I collagen fiber mesh was conducted using UV Spot Cure (SP-V: USHIO Inc., Tokyo, Japan), and irradiation intensity was measured with the above-mentioned photometer. Irradiation intensity and time were set at 0.5 mW/cm^2 and 60 min, respectively.

2.5. Multilayering electrospinning

SPU, ST-gelatin, and type I collagen were sequentially electrospun onto the same target collector (plate type or mandrel type). The spinning conditions for each polymer were set as follows (listed in the order of solvent, polymer concentration, voltage, air gap, and spinning time): (a) SPU: THF, 12.5 wt%, 25 kV, 25 cm, and 30 min; (b) ST-gelatin: HFIP, 10 wt%, 25 kV, 15 cm, and 15 min; (c) type I collagen: HFIP, 5.0 wt%, 15 kV, 15 cm, and 10 min. The flow rate was fixed at 3.0 ml/h.

2.6. Mixing electrospinning

SPU (dissolved at 15.0 wt% in THF) and PEO (dissolved at 4.0 wt% in chloroform) were simultaneously electrospun from different syringe needles (see Scheme 2). The two needles were set apart from each other by 3 cm on the disk-type electrode. The drawn polymer fibers were collected on the mandrel-type collector located immediately below 7-cm-diameter hole of the acrylic board. The mandrel was rotated and traversed in order to overlap or mix the polymer fibers landing on the mandrel. The speeds of rotation and traverse movement were set at 100 rpm and 670 mm/min, respectively. The voltage, air gap, and flow rate were set at 30 kV, 5 cm, and 1 ml/h, respectively.

2.7. Layered tubular construct

A bilayered tubular construct of SPU (outside layer) and type I collagen (inside layer) was fabricated by the above-described multilayering electrospinning process. To easily detach the fabricated bilayered tube from the mandrel-type collector, PEO was pre-electrospun onto the mandrel, i.e., first PEO, then type I collagen, and then SPU were sequentially electrospun. The spinning conditions for each polymer were set as follows (listed in the order of solvent, polymer concentration, voltage, air gap, spinning time, and mandrel rotation speed): (a) PEO: chloroform, 4.0 wt%, 15.2 kV, 15 cm, 10 min, and 1500 rpm; (b) type I collagen: HFIP, 3.0 wt%, 15 kV, 15 cm, 10 min, and 300 rpm; (c) SPU: THF, 15 wt%, 17.6 kV, 15 cm, 30 min, and 300 rpm. The flow rate and mandrel traversing speed were fixed at 3.0 ml/h and 15 mm/min, respectively.

2.8. Microscopic observation

The electrospun products of the component polymers were directly sputter-coated with platinum and their

microscopic structure was observed with a scanning electron microscope (SEM; JSM-6301F, JEOL Ltd., Tokyo, Japan) at an acceleration voltage of 8 kV. The trilayered electrospun mesh of SPU/ST-gelatin/collagen and the mixed SPU/PEO mesh were observed by a confocal laser scanning microscopy (CLSM, Radiance 2000, BIO-RAD Laboratories, Inc., Hercules, CA). Each component polymer fiber was stained with different fluorescence dyes which were premixed at 0.05% for each polymer solution [rhodamine (Sigma) for SPU and collagen; fluorescein isothiocyanate (FITC, Sigma) for ST-gelatin and PEO], and were imaged with a CLSM.

2.9. Tensile test

The tensile properties of the electrospun SPU fiber mesh and the solvent-cast SPU film used as control were characterized using a tensile tester (Rheoner II, YAMADEN Co., Ltd., Tokyo, Japan). The 0.5×2.0 cm rectangular specimen of 250 μm thickness was vertically mounted on two mechanical gripping units of the tester, leaving a 2-mm gauge length for mechanical loading. Load-deformation data were recorded every 0.2 s, at a deformation speed of 0.5 mm/s, and the stress–strain curve of the SPU film was obtained from the load-deformation curve.

3. Results

First, four polymers (type I collagen, ST-gelatin, SPU, and PEO) were individually electrospun under various formulation parameters (solvent and polymer concentration) and operation parameters (voltage, air gap, and flow rate), and the effect of the conditions on the electrospinning process and structure of electrospun constructs was assessed. Based on the optimal conditions determined, multilayered and mixed fiber meshes were fabricated, which were visualized by confocal laser scanning microscopy. Lastly, a bilayered electrospun tube composed of a collagen mesh as cell-adhesive inner layer and an SPU mesh as a mechanical and structural outer layer was constructed as a prototype of small-diameter artificial graft.

3.1. Type I collagen

Experiments with systematic changes in both formulation and operation parameters provided the optimum conditions for producing markedly thin fibers of type I collagen with diameters ranging from approximately 0.2–2 μm (Fig. 1). The effects of the parameters on the structure of the electrospun constructs were as follows. (1) Solvent: in the electrospinning using aqueous acidic solutions, the dropletlike deposition mode was predominant and fibers were hardly produced (data not shown). The use of HFIP, a volatile organic solvent with a boiling point of 61 °C, according to the work of Matthews et al. [12] who first applied HFIP to the electrospinning of collagens, enabled the production of nanofibers. (2) Polymer concentration: 1.0% collagen resulted in the significant coexistence of fibers and a beadlike structure of collagen, i.e., necklacelike structures. Collagen fibers were produced in the concentration range from 1.0 to 7.0 wt% (the maximum concentration used in this study) in HFIP. An increase in concentration under the fixed conditions of air gap (15 cm) and flow rate (3 ml/h) resulted in a significant increase in fiber diameter, which was formed at the onset voltage of the instability jet which produces nanoscale fibers. The observed mean diameters were 200 ± 60 nm for 1.0% at 16.0 kV (the onset voltage); 480 ± 60 nm for 3% at 9.2 kV; 1.25 ± 0.38 μm for 5% at 9.6 kV; and 1.86 ± 0.46 μm for 7.0% at 10.6 kV (Fig. 2a). (3) Voltage: under the fixed conditions of concentration (3%), air gap (15 cm) and flow rate (3 ml/h), a single stable jet appeared in the range of 8.0–9.2 kV and the onset of the instability jet appeared at around 9.2 kV. An increase in voltage from 9.2 kV to 25 kV did not induce a significant change in the mean diameter of the fibers (approximately 450 nm; Fig. 2b). (4) Air gap: no significant effect on fiber diameter was observed in the range between 5.0 and 20 cm under the fixed conditions of concentration (5.0%), voltage (15 kV), and flow rate (3 ml/h).

The electrospunnanofiber mesh of collagen (concentration, 5.0%; air gap, 15 cm; flow rate, 3.0 ml/h; voltage, 15.0 kV) was irradiated with UV light (0.5 mW/cm^2 at 365 nm) for 60 min. After immersion in water, a swellable but water-insoluble mesh composed of collagen fiber aggregates was formed due to intramolecular crosslinking.

3.2. Styrenated gelatin

ST-gelatin was electrospun from the HFIP solution. Regarding the effects of formulation and operation parameters on the structure of the electrospun ST-gelatin constructs, the trends observed were as similar to those of type I collagen, as follows. (1) Polymer concentration: an increase in polymer concentration under the fixed conditions of air gap (5 cm) and flow rate (3 ml/h) induced significant structural changes of the product: an increase in fiber diameter from beadlike (concentration: 2.5%), to necklacelike (5.0%), to nanofiber (7.5%) and, finally, to microfiber (10.0%) (Fig. 3) at the onset voltages of the instability jet of 11.0, 10.7, 8.5, and 7.3 kV, respectively, was observed. (2) Voltage: under the fixed conditions of concentration (7.5%), air gap (5 cm) and flow rate (3 ml/h), a single stable jet and an instability jet were induced in the range of 5.0–8.4 kV and above 8.5 kV, respectively.

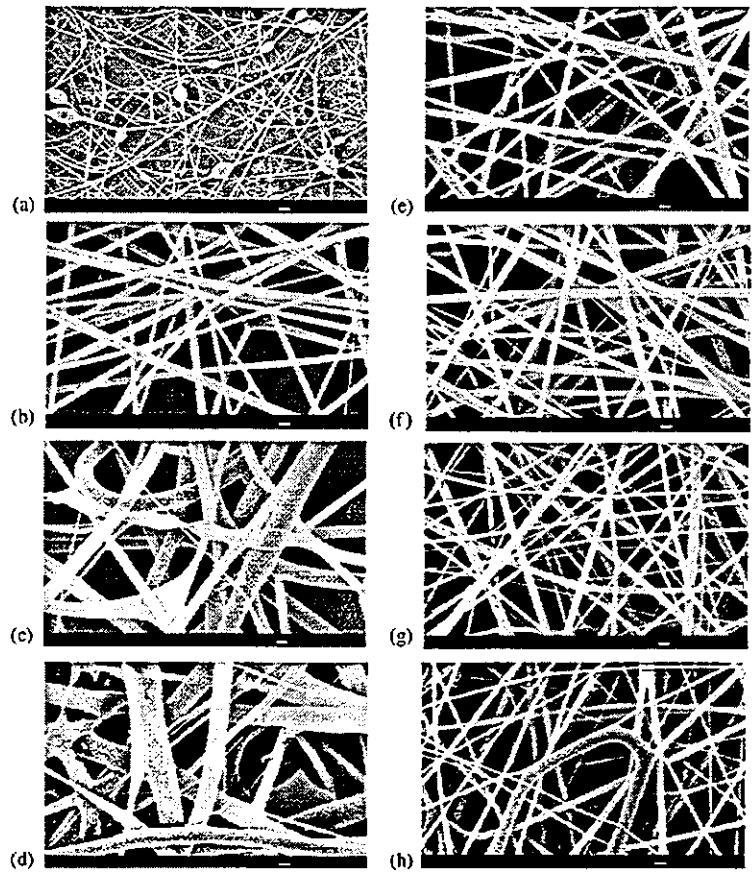

Fig. 1. Scanning electron micrograph of electrospun fibers of bovine skin type I collagen. Effect of collagen concentration on the structure of electrospun product at the onset voltage of the instability jet: (a) 1% and 16.0 kV, (b) 3% and 9.2 kV, (c) 5% and 9.6 kV, and (d) 7% and 10.6 kV. Voltage study under fixed collagen concentration (3%): (e) 10 kV, (f) 15 kV, (g) 20 kV, (h) 25 kV. Air gap: 15 cm. Flow rate: 3 ml/h. Scale bars: 1 μm.

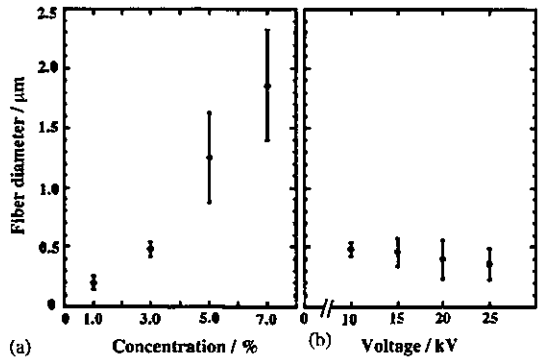

Fig. 2. Mean diameter of electrospun type I collagen as a function of (a) collagen concentration and (b) voltage. Error bars show standard deviations.

The electrospun nanofiber mesh of ST-gelatin [prepared from the mixed HFIP solution of ST-gelatin (concentration 7.5%) and camphorquinone (1.0 wt% to the weight of gelatin); air gap, 5 cm; flow rate, 3 ml/h; voltage, 10.0 kV] was irradiated with visible light (50 mW/cm^2 at 568 nm) for 10 min. After immersion in water, a swellable but water-insoluble mesh was formed due to photopolymerization and intramolecular crosslinking.

3.3. Segmented polyurethane

The trends in the structure of the electrospun SPU constructs with varying formulation and operation parameters were similar to those of collagen and ST-gelatin. An example is shown in Fig. 4a in which thin fibers with a typical diameter of around several micros were generated (solvent, THF; concentration, 15 wt%; voltage, 25 kV; air gap, 30 cm; flow rate, 3 ml/h). Occasionally, two fibers were fused or bonded at their contact sites (Figs. 4b and c). Such bonding between fibers may affect the elasticity of the electrospun SPU fiber mesh as well as the maintenance of the mesh structure under periodically loaded stress field. The tensile measurement test showed that lower tensile stress caused much greater elongation of the electrospun meshes than that of the solvent-cast film of

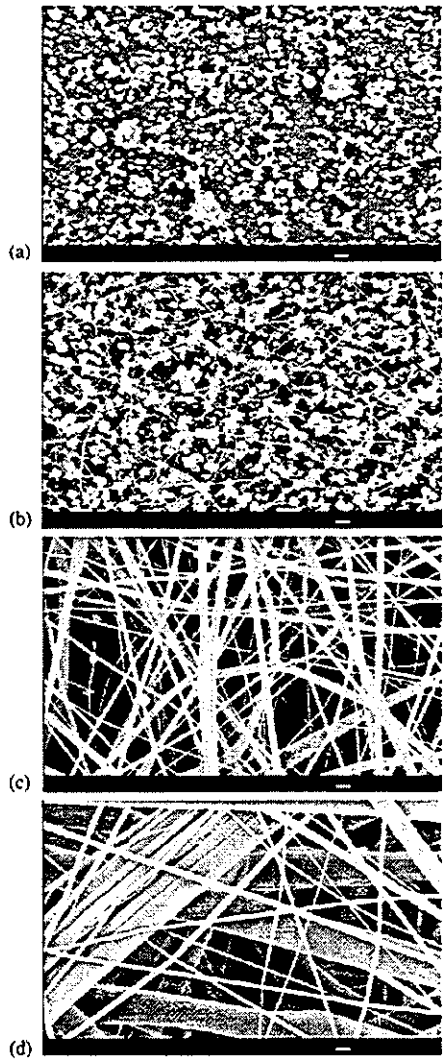

Fig. 3. Scanning electron micrograph of electrospun fibers of ST-gelatin. Concentration study at the onset voltage of the instability jet: (a) 2.5% and 11.0 kV, (b) 5.0% and 10.7 kV, (c) 7.5% and 8.5 kV, (d) 10.0% and 7.3 kV. Air gap: 5 cm. Flow rate: 3 ml/h. Scale bar: 1 μm.

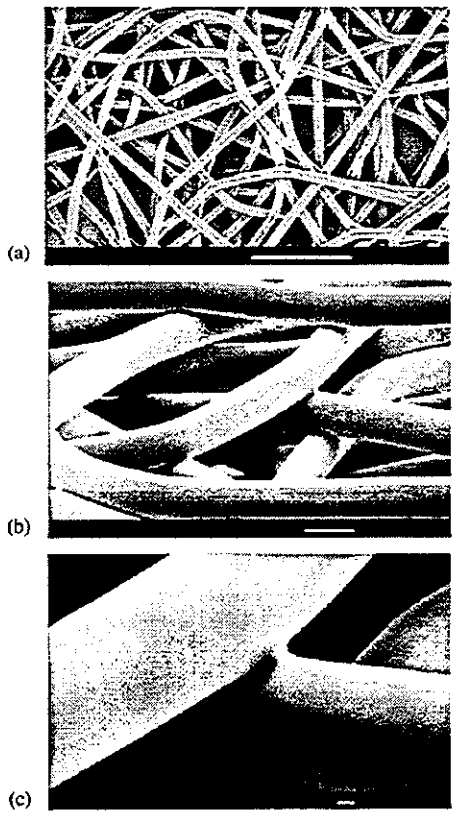

Fig. 4. Scanning electron micrograph of electrospun fibers of SPU. Concentration: 15%. Voltage: 25 kV. Air gap: 30 cm Flow rate: 3 ml/h. Scale bars: (a) 100 μm and (b, c) 1 μm.

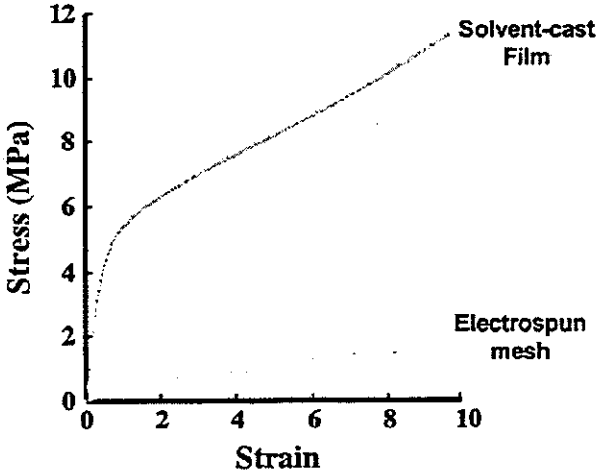

Fig. 5. Stress–strain curves for electrospun film and solvent-cast film of SPU.

approximately the same thickness (ca. 250 μm) (Fig. 5). Young's moduli of the ELSP mesh and solvent-cast film were determined from the initial slope in Fig. 5 to be 0.59 and 10.4 MPa, respectively. From the size (30 mm × 40 mm × 250 μm) and weight of the film or mesh (0.4047 g for the film and 0.0847 g for the mesh), the porosity of the electrospun mesh was determined as 79.1%.

3.4. Poly(ethylene oxide)

For the optimization of the formulation parameters of PEO electrospinning, water and chloroform were tested as the electrospinning solvent. PEO fibers electrospun from the aqueous solution fused with each other due to the slow evaporation of water. Using chloroform as the solvent, the electrospun PEO fibers were clearly kept (diameter: several to several tens micrometer) and a fine fiber mesh was formed. The

trends of the structure of the electrospun PEO constructs with varying formulation and operation parameters were similar to those of collagen, ST-gelatin, and SPU.

3.5. Multilayering electrospinning

Using the above-described component polymers under the individually defined conditions, multilayering ELSP was performed according to the method shown in Scheme 1, i.e., sequential spinning. To distinguish and visualize the layered structure composed of individual component polymers, each polymer solution was dissolved with a fluorescence dye and the layered structure was visualized by CLSM. SPU (mixed with rhodamine), ST-gelatin (mixed with FITC), and type I collagen (mixed with rhodamine) were sequentially electrospun onto the plate-type collector. After the ST-gelatin fiber mesh was formed, visible light was irradiated onto it to produce crosslinked fibers which are swellable but insoluble in water. For type I collagen, UV light was used for irradiation to produce swellable but insoluble fiber aggregates. Fig. 6-1 shows the CLSM images of the electrospun layered meshes. Planes confocally scanned at 10 μm height intervals showed that the SPU, ST-gelatin, and collagen layers were segregated and hierarchically positioned in the order of the vertical direction of the meshes. A mixing zone appears to exist between two adjacent layers. The multilayered nano- and microfiber meshes were fabricated by applying the sequential electrospinning technique.

3.6. Mixing electrospinning

Mixing ELSP was performed using SPU and PEO, which were simultaneously electrospun from different syringe needles on the rotating and traversing mandrel-type collector. From preliminary experiments, the projected polymer solutions were found to repel each other due to the electrostatic repulsion of charges on the surfaces of the projected jets [21,22], when these two polymer solutions were simultaneously electrospun on the same region of the target collector. In particular, such repulsion was found to be strong between the instability jets, thus they inevitably landed on the markedly distant areas on the collector and could not be mixed with each other. To mix the electrospun fibers, two improvements were required: one is to confine the target area of the grounded collector using the insulated acrylic board with a 7-cm-diameter hole (see Scheme 2), which was effective in bringing closer the landing regions of the two jets over the narrow area of the collector. The other is to use the moving collector with a high-speed rotation and traverse movement, which results in the coarse and rapid overlapping of the nano- and microfiber meshes. Through these setups, two kinds of polymer fibers were electrospun on the surface of the moving collectors, which were deposited in different regions inside the confined area on the moving

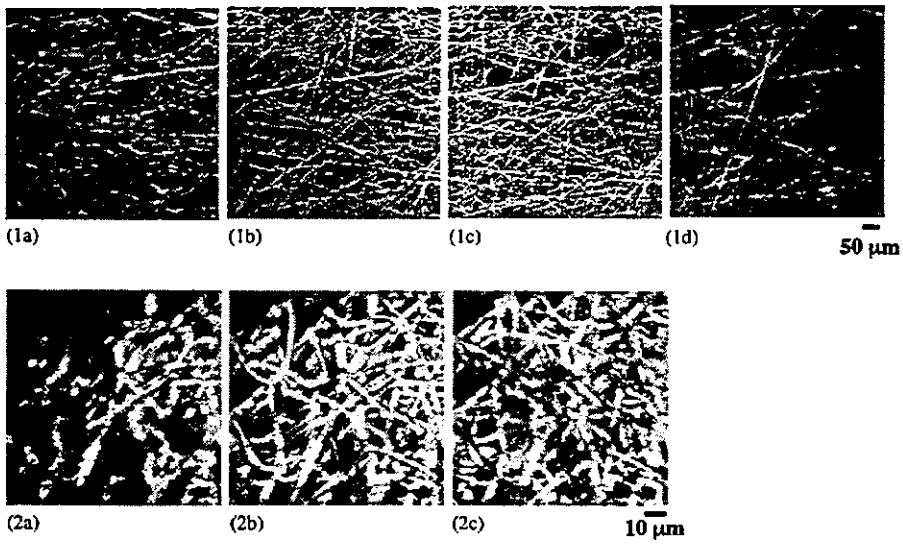

Fig. 6. Confocal laser scanning micrographs of trilayered fiber mesh of collagen/ST-gelatin/SPU (1) and mixed fiber mesh of SPU/PEO (2). (1a) Rhodamine-stained SPU electrospun fibers observed in the bottom region of the trilayered mesh. (1b) Observation at the 10 μm-upper region than (1a). (1c) FITC-stained ST-gelatin electrospun fibers observed at the 10 μm-upper region than (1b). (1d) Rhodamine-stained type I collagen electrospun fibers observed at the 10 μm-upper region than the (1c). (2a) Bottom region of the mixed fiber mesh. SPU and PEO were stained with rhodamine and FITC, respectively. (2b) Middle region of the mesh observed at the 4 μm-upper region than (2a). (2c) Top region of the mesh observed at the 4 μm-upper region than (2b).

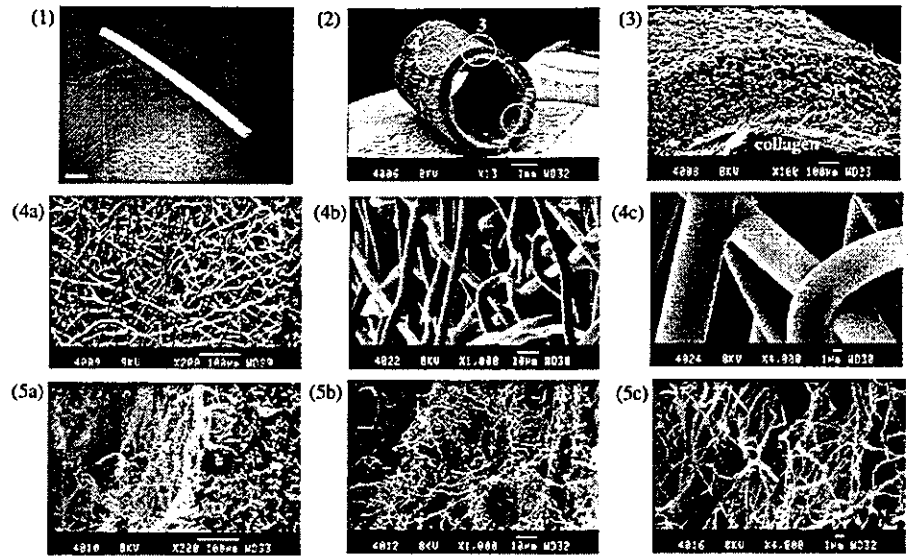

Fig. 7. Fabricated bilayered tubular construct of SPU/collagen. (1) Appearance of the tube. Scale bar: 1 mm. (2) Scanning electron micrograph of the tube. (3) Magnified image of region 3 in photo (2). (4a–c) Magnified images of the outer layer of region 4 in photo (2). (5a–c) Magnified images of the inner layer of region 5 in photo (2).

mandrel-type collector but forcibly overlapped by the movement of the collector. Fig. 6-2 shows the confocal microscopy image of the overlapping regions (middle portion of formed meshes) of these electrospun SPU (stained with rhodamine) and PEO (stained with FITC) fibers. The observation for confocally scanned planes at 4 μm height intervals evidenced that two different microfiber meshes are mixed. Thus, the mixing of the electrospun nano- and microfibers was attained using two needles, a confined region of the collector, and a moving collector.

3.7. *Layered tubular construct*

Using a rotating and traversing mandrel-type collector (Scheme 2), a thin-layered PEO mesh was first formed on the mandrel, then type I collagen was electrospun to form a layered nanofiber mesh, and finally, a thick SPU mesh was electrospun. In order to largely differentiate the fiber diameters of collagen and SPU in the tubular construct compared with those fibers in the multilayered mesh described above, concentrations were appropriately changed from those used for the multilayered meshes. Voltage and air gap conditions were also regulated suitable for producing instable jets on the mandrel-type collector. The first deposited layer of the PEO microfiber mesh did not exhibit significant adhesion to the second collagen mesh, and remained on the collector when the collagen/SPU tube was pulled out from the collector in air (data not shown). After the removal of the tubular electrospun product from the mandrel (20 cm in length and 3 mm in outer diameter), a bilayered tube (10 cm in length, 3 mm in inner diameter, and ca. 500 μm in thickness) was formed. An image of the entire tube, its SEM image and a magnified image of region 3 in the SEM image are shown in Fig. 7-1, 7-2 and 7-3, respectively. SPU microfiber meshes and thin-layered type I collagen nanofiber meshes are shown in Fig. 7(4a-c) and (5a-c), respectively.

4. Discussions

ELSP has recently attracted considerable attention in line with constructing a nanofiber-based scaffold for artificial and tissue-engineered devices, in which nano- to microfiber meshes formed from a single-component polymer serve as a cell-adhesive matrix or a structural scaffold. More complex or higher-ordered structured mesh on the mesoscopic scale may add higher functional value to the devices incorporated with ELSP meshes. To this end, we devised two techniques: multilayering and mixing of different polymeric fiber meshes.

As for the multilayering process, a sequential ELSP enables the production of hierarchical meshes through the layer-by-layer process as was clearly visualized with a CLSM for trilayered meshes composed of three (bio)polymers (Fig. 6). The three-layered sheet exemplified a prototype model (Fig. 6a): hierarchically placed in the vertical direction are an elastomeric SPU microfiber layer as a structural component, a photocrosslinked ST-gelatin nanofibrous hydrogel layer as a drug-releasing reservoir (for instance, heparin as an anticoagulant, growth factors for recruitment and proliferation of vascular cell types via transmural migration and capillary ingrowth will be incorporated in the hydrogel),

and a UV-crosslinked collagen nanofiber layer as a cell-adhesive matrix. The drug-releasing properties of the photocrosslinked ST-gelatin hydrogel were reported in our previous study [20]. When the ELSP meshes composed of water-soluble biopolymers such as collagen and gelatin are formed, such meshes cannot be used for tissue-engineered devices by themselves because they are dissolved away while in contact with tissue fluid or blood. Postelectrospinning procedures leading to crosslinking or insolubilization in water are required in biomedical applications. Matthews et al. conducted the crosslinking of electrospun collagens in glutaraldehyde vapor [12], and found that the crosslinked collagennanofibers thus formed can be used as a cell-adhesive matrix. Transmission electron microscopic observations showed that the electrospun collagen nanofibers exhibit the 67 nm banding typical for assembled native collagen, indicating that denaturation of collagen does not occur [12]. In the present experiment, the UV crosslinking of collagen and visible-light-induced crosslinking of ST-gelatin in the presence of visible-light-induced radical generators such as camphorquinone were also effective for insolubilization. Both insolubilized biopolymers swelled under water but were cell adhesive (data not shown).

When such a sequential multilayering ELSP is performed on the rotating mandrel-type collector, the biological design of an artificial graft wall may be feasible. The methodology was applied to the design of the multilayered graft wall, as exemplified by the SPU/collagen-bilayered tube (Fig. 7). As for the electrospun artificial grafts [18,23,24], Annis et al. pioneered the fabrication of a SPU-fiber-based graft, which was fabricated on the rotating and traversing movable mandrel to incorporate the mechanical design criteria for compliance matching with native arteries [18]. They have found that the electrospun SPU-based artificial vessel enables the regeneration of a viable and normal neoinitima upon experimental implantation into an animal's arteries and responds to the arterial stress field, thus achieving compliance matching with adjacent native arteries. In the present article, we utilized a custom-made mandrel capable of high-speed rotation and traverse movement, coupled with sequential electrospinning. A bilayered tubular construct was spatially designed to have a thin collagen mesh as a luminal layer and a thick SPU mesh as a compliant scaffold. Such hierarchically designed artificial graft may provide compliance matching with native arteries, cell and tissue ingrowth, and transient antithrombogenicity in the early phase of implantation, which will be reported in the near future.

As for the mixing ELSP technique, two different fibers can be placed close to each other when the alternating deposition speed of the different fibers per unit area is sufficiently high and each fiber is sufficiently thinly deposited in a certain moment in the vertical direction under the condition of sufficiently high-speed movement of the collector surface on the rotating and traversing mandrel. Such kind of deposited state of fibers may be defined as "mixing", although no entanglement of two different fibers occurs in principle. If the deposition of each fiber is thick and dense in the vertical direction under the condition of slow movement of the collector, layer-by-layering is formed. In such case, mixing is limited only at the interface of the two deposited fiber meshes. In this study, the mixed microfiber mesh of SPU and PEO was fabricated, in which PEO was employed as a leaching polymer to create micropores or microvoids for cells from a surrounding tissue to migrate and reside in the luminal surface of the fabricated vascular graft after the PEO fibers have dissolved in water; this will be reported in the near future. The electrospun mesh generally exhibits much less porosity than the conventional tissue-engineering scaffold such as highly porous microstructure and is required to appropriately create the interconnected microvoid structure of the electrospun mesh for cell ingrowth. For this task, the methods for creating the microvoid inside the mesh should be devised. As one of such devises, the above-proposed fiber-leaching method using mixing electrospinning may be applicable.

5. Conclusion

In this study, two new electrospinning techniques, multilayering electrospinning and mixing electrospinning, were devised to design a mesoscopically ordered structure of the matrices and scaffolds composed of nano- and microscale fiber meshes for artificial and tissue-engineering devices. A trilayered electrospun nano/microfiber mesh (type I collagen, ST-gelatin, and SPU) and a mixed electrospun-fiber mesh (SPU and PEO) were substantiated. A bilayered tubular construct composed of a thick SPU microfiber mesh as an outer layer and a thin type I collagen nanofiber mesh as an inner layer was fabricated as a prototype scaffold of artificial grafts. Mesoscopic spatial depositions and structural constructs by devised electrospinning techniques and the post-spinning process proposed in this study may find new applications in tissue engineering.

Acknowledgements

The authors thank Dr. T. Kanemaru of Faculty of Medicine, Kyushu University, for his help in the SEM observation. This work was supported by a Grant-in-Aid for Scientific Research from the Ministry of Health, Labour and Welfare (MHLW) of Japan, and in part by a Grant-in-Aid for Scientific Research and for the

Creation of Innovations through Business-Academic-Public Sector Cooperation from the Ministry of Education, Culture, Sports, Science, and Technology (MEXT) of Japan.

References

[1] Kreis T, Vale R, editors. Extracelluar matrix, anchor, and adhesion proteins, 2nd ed. New York: Oxford University Press; 1999. Part 3.
[2] Kadler KE, Holmes DF, Trotter JA, Chapman JA. Collagen fibril formation. Biochem J 1996;316:1–11.
[3] Goodman SL, Sims PA, Albrecht RM. Three-dimensional extracellular matrix textured biomaterials. Biomaterials 1996;17:2087–95.
[4] Ma PX, Zhang R. Synthetic nano-scale fibrous extracellular matrix. J Biomed Mater Res 1999;46:60–72.
[5] Zhang R, Ma PX. Synthetic nano-fibrillar extracellular matrices with predesigned macroporous architectures. J Biomed Mater Res 2000;52:430–8.
[6] Tan W, Krishnaraj R, Desai TA. Evaluation of nanostructured composite collagen-chitosan matrices for tissue engineering. Tissue Eng 2001;7:203–10.
[7] Stitzel JD, Bowlin GL, Mansfield K, Wnek GE, Simpson DG. Electrospraying and electrospinning of polymers for biomedical applications. Poly(lactic-*co*-glycolic acid) and poly(ethylene-*co*-vinylacetate). 32nd International SAMPE Technical Conference 2000. p. 205–11.
[8] Huang L, Apharian RP, Chaikof EL. High-resolution analysis of engineered type I collagen nanofibers by electron microscopy. Scanning 2001;23:372–5.
[9] Boland ED, Wnek GE, Simpson DG, Pawlowski KJ, Bowlin GL. Tailoring tissue engineering scaffolds using electrostatic processing techniques: a study of poly(glycolic acid) enectrospinning. J Macromol Sci—Pure Appl Chem 2001;A38:1231–43.
[10] Li WJ, Laurencin CT, Caterson EJ, Tuan RS, Ko FK. Electrospun nanofibrous structure: a novel scaffold for tissue engineering. J Biomed Mater Res 2002;60:613–21.
[11] Deitzel JM, Kosik W, McKnight SH, Beck Tan NC, DeSimone JM, Crette S. Electrospinning of polymer nanofibers with specific surface chemistry. Polymer 2002;43:1025–9.
[12] Matthews JA, Wnek GE, Simpson DG, Bowlin GL. Electrospinning of collagennanofibers. Biomacromolecules 2002;3:232–8.
[13] Yoshimoto H, Shin YM, Terai H, Vacanti JP. A biodegradable nanofibers scaffold by electrospinning and its potential for bone tissue engineering. Biomaterials 2003;24:2077–82.
[14] Kenawy ER, Layman JM, Watkins JR, Bowlin GL, Matthews JA, Simpson DG, Wenk GE. Electrospinning of poly(ethylene-*co*-vinyl alcohol) fibers. Biomaterials 2003;24:907–13.
[15] Formhals A. Apparatus, process for making artificial threads. Patent 1929, GB364780.
[16] Doshi J, Reneker DH. Electrospinning process and applications of electrospun fibers. J Electrostatics 1995;35:151–60.
[17] Cloupeau M, Prunet-Foch B. Electrostatic spraying of liquids: main functioning modes. J Electrostatics 1990;25:165–84.
[18] Annis D, Bornat A, Edwards O, Higham A, Loveday B, Wilson J. An elastmeric vascular prosthesis. Trans Am Soc Artif Intern Organs 1978;24:209–14.
[19] Nakayama Y, Matsuda T. Photocurable surgical tissue adhesive glues composed of photoreactive gelatin and poly(ethylene glycol) diacrylate. J Biomed Mater Res (Appl Biomater) 1999;48: 511–21.
[20] Okino H, Nakayama Y, Tanaka M, Matsuda T. In situ hydrogelation of photocurable gelatin and drug release. J Biomed Mater Res 2002;59:233–45.
[21] Hohman MM, Shin M, Rutledge G, Brenner MP. Electrospinning and electrically forced jets. I Stability theory. Phys Fluid 2001;13:2201–20.
[22] Hohman MM, Shin M, Rutledge G, Brenner M. Electrospinning,electrically forced jets. II. Applications. Phys Fluid 2001;13: 2221–36.
[23] How TV, Clarke RM. The elestic properties of a polyurethane arterial prosthesis. J Biomech 1984;8:597–608.
[24] Zhang Z, Marois Y, Guidon RG, Bull P, Marois M, How T, Laroche G, King MW. Vascugraft polyurethane arterial prosthesis as femoro-popliteal and femoro-peroneal bypass in humans: pathological, structural and chemical analyses of four excised grafts. Biomaterials 1997;18:113–24.

Available online at www.sciencedirect.com
SCIENCE DIRECT®
Biomaterials 26 (2005) 3929–3939
Biomaterials
www.elsevier.com/locate/biomaterials

Electrospun nano- to microfiber fabrics made of biodegradable copolyesters: structural characteristics, mechanical properties and cell adhesion potential

Il Keun Kwon, Satoru Kidoaki, Takehisa Matsuda*

Department of Biomedical Engineering, Graduate School of Medicines, Kyushu University, 3-1-1 Maidashi, Higashiku, Fukuoka city, Fukuoka 812-8582, Japan

Received 20 May 2004; accepted 14 October 2004

Abstract

Nano- to micro-structured biodegradable poly(L-lactide-*co*-ε-caprolactone) (PLCL) fabrics were prepared by electrospinning. Electrospun microfiber fabrics with different compositions of PLCL (mol% in feed; 70/30, 50/50, and 30/70), poly(L-lactide) (PLL) and poly(ε-caprolactone) (PCL) were obtained using methylene chloride (MC) as a solvent. The PLL microfiber exhibited a nanoscale-pore structure with a pore diameter of approximately 200–800 nm at the surface and subsurface regions, whereas such a surface structure was hardly observed in other polymers containing CL. The microfiber fabric made of PLCL 50/50 was elastomeric. Nanoscale-fiber fabrics with PLCL 50/50 (approx. 0.3 or 1.2 μm in diameter) were electrospun using 1,1,1,3,3,3-hexafluoro-2-propanol (HFIP) as a solvent. Mercury porosimetry showed that the decrease in the fiber diameter of the fabric decreased porosity, but increased fiber density and mechanical strength. Human umbilical vein endothelial cells (HUVECs) were adhered well and proliferated on the small-diameter-fiber fabrics (0.3 and 1.2 μm in diameter), both of which are dense fabrics, whereas markedly reduced cell adhesion, restricted cell spreading and no signs of proliferation were observed on the large-diameter-fiber fabric (7.0 μm in diameter). The potential biomedical application of electrospun PLCL 50/50 was discussed.

Keywords: Electrospinning; Nanofibers; Microfibers; Dielectric constant; Human umbilical vein endothelial cell (HUVEC)

1. Introduction

Various micropored polymeric scaffold fabrication techniques of generating interconnected pores on a few tenths to several hundreds of micrometer scale, which include fiber bonding [1], solid free-form fabrication [2], and salt extraction [3], have been widely used in tissue engineering. Recent studies showed that cells recognize nanometric topologies of fibrous or microporous structure. Such a nanoscale structure geometrically or topologically mimics the native state of extracellular matrix (ECM) biomacromolecules in living tissues, such as collagen, hyaluronic acid, laminin, and fibronectin and their complex supramolecular assemblies [4,5]. The fabrication and design of submicron- to nanoscale structural architectures have received much attention in medical applications [6–10].

Electrospinning is a fiber spinning technique driven by a high-voltage electrostatic field using a polymeric solution or liquid that produces polymer fibers with diameters ranging from several micrometers down to 100 nm or less [11,12]. The variables controlling the behavior of the electrified fluid jet during electrospinning can be divided into fluid properties and operating parameters. The relevant fluid properties are viscosity (η), conductivity (K), dielectric constant (ε), boiling point (bp), and surface tension (γ). The operating parameters are flow rate (Q), applied electric potential

*Corresponding author. Tel.: +81 92 642 6210; fax: +81 92 642 6212.
E-mail address: matsuda@med.kyushu-u.ac.jp (T. Matsuda).

0142-9612/$ - see front matter © 2004 Elsevier Ltd. All rights reserved.
doi:10.1016/j.biomaterials.2004.10.007

(V), and the distance between the tip and the collector called air gap (d) [11,12].

In the design of a provisional scaffolding material for the fabrication of engineered tissues, a candidate polymer should possess appropriate mechanical properties, which are suitable for target applications, and its degradation products during implantation should be metabolic substances produced by the living body, thus guaranteeing inherent nontoxicity. Over the past years, hydrolyzable and biocompatible copolymers of ε-caprolactone (CL) and L-lactide (LL) have been of great interest for medical applications [13,14]. Polylactide (PLL) is a crystallizable hard and brittle material, whereas poly(ε-caprolactone) (PCL) is a semicrystalline material with rubbery properties [3,15]. Copolymers of LL and CL (PLCL) exhibit various mechanical properties, depending on their composition [16]. For example, the high-molecular-weight equimolar copolymer PLCL 50/50 is a biodegradable elastomer [17].

In this study, a series of high-molecular-weight PLCLs of different compositions was prepared by ring-opening copolymerization. As a continuation of our series of studies on electrospinning technology in biomedical application, the followings were studied in this article: (1) The copolymer composition dependency on the physical state and mechanical properties of electrospun fibers. (2) Internal structural features including and mechanical integrity of electrospun fabrics made of the equimolar copolymer, which were prepared using different solvents under different operation conditions, were evaluated in terms of their fiber diameter, and porosity, and (3) the dependency of cell adhesion and proliferation potentials on surface fiber density.

2. Materials and methods

2.1. Materials

All the solvents and reagents used were purchased from either Wako Pure Chemical Industries Ltd. (Osaka, Japan) or Sigma-Aldrich Japan, Inc. (Tokyo, Japan). L-lactide (LL) was recrystallized from ethyl acetate. ε-caprolactone (CL) was purified by drying over calcium hydride (CaH_2) for 24 h at room temperature and then distilled it under a reduced pressure (approximately 0.3 mmHg) at 55 °C. Stannous octoate ($Sn(Oct)_2$) was purified by vacuum distillation at 175 °C (ca. 0.2 mmHg). Toluene was thoroughly dried by distillation over CaH_2. The other solvents and reagents were of extra pure grade and used as received.

2.2. Copolymerization

The equimolar copolymerization of PLCL was carried out in a 50-mL glass ampoule containing 14.4 g (0.1 mol) of LL and 11.4 g (0.1 mol) of CL. 0.005 g (1.3×10^{-5} mol) of $Sn(Oct)_2$ diluted with dried toluene was added to the ampoule using a syringe. The ampoule was heated under a reduced pressure to remove toluene, and then sealed by heating with a torch under vacuum. The copolymerization was carried at 150 °C in a silicone oil bath for 24 h. The copolymer was obtained by precipitation in methanol and vacuum-dried for 48 h at room temperature. Irrespective of the composition of PLCL, the yield was found to be almost 100%. The process conditions used for the other feed ratios of LL to CL (100/0, 70/30, 30/70, and 0/100 mol/mol) were the same as those used for PLCL 50/50.

2.3. PLCL copolymer characterizations

Copolymer compositions were calculated from ^{1}H-NMR spectra, which were recorded on JNM-AL300 (JEOL, Tokyo, Japan). Chemical shifts are given in δ from Me_4Si as an internal standard. The number-average molecular weight (Mn) of each polymer was determined using a gel permeation chromatograph (GPC) (Waters 410, Milford, MA) fitted with microstyragel columns and calibrated with narrow polystyrene standards (Aldrich). Chloroform was used as the mobile phase at a flow rate of 1.0 ml/min at 30 °C.

2.4. Electrospinning apparatus

The setup of our electrospinning apparatus was reported in our previous work [18]. Briefly, it consisted of a high-voltage-power supply (HSP-30k-2; Nippon Stabilizer Inc., Osaka, Japan), an infusion pump (model 22; Harvard Apparatus Inc., Holliston, MA), a glass syringe equipped with a stainless-steel blunt-ended needle [outer diameter, 1.0 mm; inner diameter, 0.8 mm], and an aluminum plate-type collector.

2.5. Electrospinning

For the electrospun microfiber fabrics, a series of PLCL solutions was prepared by dissolving the copolymers in methylene chloride (MC) at a concentration of 4–11 wt%, depending on the composition of copolymer. The polymer solution was delivered at a constant flow rate (10 ml/h) using an infusion pump to the stainless-steel blunt-ended needle with an air gap between the metal collector and the needle tip of 30 cm at a driving voltage of 12.5 kV (Table 2). For the electrospun submicron or nanofiber fabrics with PLCL 50/50, the conditions were as follows: solvent, 1,1,1,3,3,3-hexafluoro-2-propanol (HFIP, Sigma Chemical Co., St. Louis, MO); polymer concentration, 3 wt%; flow rate, 5 or 10 ml/h; air gap, 20 cm; and driving voltage, 15 or 30 kV (Table 3).

2.6. Scanning electron microscopy

The electrospun products of PLCL were sputter-coated with platinum, and the microscopic structure was observed by scanning electron microscopy (SEM, JSM-840A, JEOL Ltd., Tokyo, Japan) at an acceleration voltage of 8 kV. The mean fiber diameters of the electrospun PLCL fabrics were calculated using 20 fibers seen on each SEM image.

2.7. Porosimetry

Pore diameter distribution, total pore volume, and the porosity of the electrospun PLCL 50/50 nano- to microfiber fabrics (approx. 140 μm thickness) were measured using a mercury intrusion porosimeter (Poresizer 9320, Micromeritics Instrument Co., Norcross, GA) in mercury intrusion under an increasing pressure from 100 kPa to 207 MPa, which was carried out at Toray Research Center (Tokyo, Japan). The determination of porosity was based on the relationship between the applied pressure and the pore diameter into which mercury intrudes, according to the Washburn equation:

$$D = (-4\gamma \cos\theta)/P$$

where P is the applied pressure, D is the pore diameter, γ is the surface tension of the mercury (484 mN m^{-1}) and θ is the contact angle between mercury and the pore wall, taken as 141.3° [19].

2.8. Tensile test

The uniaxial tensile properties of the electrospun PLCL nano- to microfiber fabrics (5 × 20 × 0.14 mm) were determined using a tensile tester (Rheoner II, Yamaden Co. Ltd., Tokyo, Japan). The stress–strain curves of the samples were obtained from the load-deformation curves recorded at a stretching speed of 0.5 mm/s.

2.9. Cell culture examination

The electrospun fabrics (10 × 10 mm^2), sterilized with 70% ethanol, followed by washing with phosphate buffered saline (PBS) and subsequent air-drying, were placed on the bottom of a 24-well culture dish (Corning, NY). Human umbilical vein endothelial cells (HUVECs, obtained from the American Type Culture Collection, 5 × 10^4 cells/cm^2) were seeded and cultured in the dish in an endothelial cell basal medium 2 (EC-2, Clonetics, Walkersville, MD) supplemented with 5% fetal bovine serum (FBS, Life Technologies, Rockville, MD) and 0.94% microvascular endothelial cell medium-2 (EGM-2 MV, Clonetics), which contained a human endothelial growth factor, a human fibroblast growth factor, a human epidermal growth factor, insulin-like growth factor I, ascorbic acid, and hydrocortisone acetate, at 37 °C in a humidified 5% CO_2 atmosphere. The number of cells on the electrospun fabrics was determined using a hematocytometer after detaching the cells from the fabrics using 0.1%-trypsin (Life Technologies).

2.10. Statistical analysis

All the quantitative values were expressed as a mean ± standard deviation. Statistical analysis was carried out using an ANOVA with a Scheffé test post hoc ($p < 0.05$) using Statview for Windows (SAS Institute Inc., Copyright 1992–1998) version 5.0.

3. Results

3.1. Electrospun PLCL microfiber fabrics

A series of PLCL copolymers with different copolymer composition was synthesized by ring-opening (co)polymerization in the presence of Sn(Oct)$_2$ in bulk at 150 °C (Scheme 1). Table 1 summarizes the reaction conditions, feed monomer compositions, copolymer compositions, molecular weights and the polydispersities of their copolymers. Irrespective of the type of (co)polymer, the yield was approximately 92–97%. The compositions of the copolymers were determined by ^{1}H-NMR spectroscopy (Fig. 1). The methine protons of the lactide unit appeared at δ 5.1–5.2 (Fig. 1a, a′), which can be ascribed to the sequence distribution of the lactyl and caproyl units. The methylene protons of the caproyl unit adjacent to the ester group appeared at δ 4.0–4.2 (Fig. 1c, c′) and δ 2.3–2.5 (Fig. 1g, g′). The copolymer compositions determined from these relative intensities were almost identical to those of the initial feed compositions, as expected from the fact that the reaction was completed at almost full conversion. The

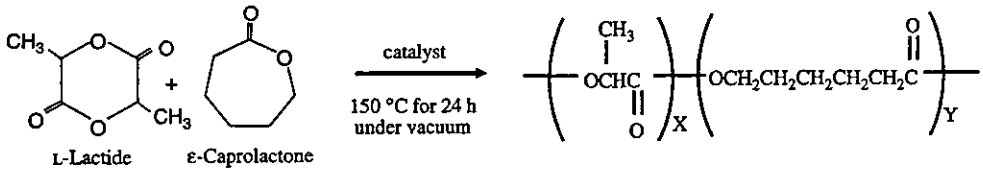

L-Lactide ε-Caprolactone

Scheme 1. Schematics of preparation of poly(L-lactide-*co*-ε-caprolactone) (PLCL).